MITIGATING MULTIMODAL HALLUCINATIONS VIA GRADIENT-BASED SELF-REFLECTION

Anonymous authors
Paper under double-blind review

ABSTRACT

Multimodal large language models achieve strong performance across diverse tasks but remain prone to hallucinations, where outputs are not grounded in visual inputs. This issue can be attributed to two main biases: text–visual bias, the overreliance on prompts and prior outputs, and co-occurrence bias, spurious correlations between frequently paired objects. We propose Gradient-based Influence-Aware Constrained Decoding (GACD), an inference-based method, that addresses both biases without auxiliary models, and is readily applicable to existing models without finetuning. The core of our approach is bias estimation, which uses first-order Taylor gradients to understand the contribution of individual tokens—visual features and text tokens—to the current output. Based on this analysis, GACD mitigates hallucinations through two components: (1) suppressing spurious visual features correlated with the output objects, and (2) rebalancing cross-modal contributions by strengthening visual features relative to text. Experiments across multiple benchmarks demonstrate that GACD effectively reduces hallucinations and improves the visual grounding of MLLM outputs.

1 INTRODUCTION

Recent advances in Multimodal Large Language Models (MLLMs) have demonstrated remarkable capabilities in producing coherent and context-aware content across a wide range of domains (Bai et al., 2023; Dai et al., 2023; Chen et al., 2024b; Liu et al., 2024a; Ye et al., 2024). Despite their impressive advancements, these models remain prone to hallucination, wherein the generated text is not faithfully grounded in the visual modality (Rohrbach et al., 2018; Li et al., 2023b). This limitation poses a critical barrier to establishing trust in the outputs of MLLMs.

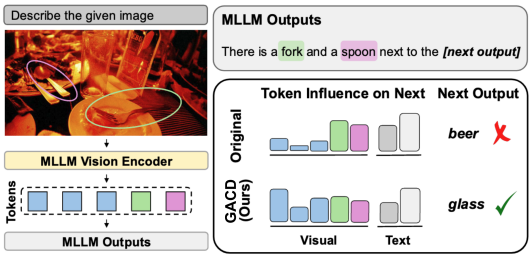

Figure 1: Overview of our influence-aware constrained decoding framework, which mitigates hallucinations by regulating token-level influence. It reduces text–visual bias by enhancing visual token influence (blue bars) in alignment with the most influential text inputs— prompts (gray) or previous outputs (white). It further mitigates co-occurrence bias through anchor-specific suppression, selectively suppressing visual tokens (green, magenta) anchored to previously emitted nouns.

The hallucinations observed in MLLMs can be largely attributed to two fundamental biases (Kang & Choi, 2023; Li et al., 2023b; Kim et al., 2024). **Text-visual bias** refers to the excessive reliance on textual information—such as the input prompt and previously generated outputs—while neglecting the visual modality during generation. This bias becomes particularly pronounced in longer sequences, where MLLMs tend to depend more heavily on prior text and increasingly disregard visual cues (Zhou et al., 2023b; Favero et al., 2024). **Co-occurrence bias** arises from spurious statistical correlations embedded in the training data, which lead models to erroneously predict the presence of non-existent objects based on their frequent co-occurrence with observed objects in the visual inputs (Li et al., 2023b). This bias is particularly challenging to mitigate, and existing approaches largely rely on statistical priors rather than offering statistically agnostic solutions (Kang & Choi, 2023; Zhou et al., 2023a).

Existing efforts to mitigate hallucinations in MLLMs can be broadly categorized into inference-based methods, which operate at the decoding stage (Chen et al., 2024a; Favero et al., 2024; Leng et al., 2024; Park et al., 2024; Woo et al., 2024), and training-based approaches, which intervene during model optimization (Ben-Kish et al., 2023; Chen et al., 2023b; Kang & Choi, 2023; Sun et al., 2023; Jiang et al., 2024; Yue et al., 2024). Inference-based approaches are valued for their cost-effectiveness, as they avoid the need for additional data collection, data bias examination, or extensive model retraining. However, these methods offer limited insight into the severity of underlying biases, leaving the root causes of hallucination insufficiently understood. In addition, some inference-based methods rely on auxiliary models—such as segmentation networks Chen et al. (2024a), detection systems Kan et al. (2024) , or even additional MLLMs (Radford et al., 2021; Deng et al., 2024; Xing et al., 2024)—which undermine their purported cost-effectiveness.

Another limitation of existing methods lies in their lack of granularity when adjusting the underlying biases in MLLMs. Most approaches rely on heuristically tuned priors, which vary across datasets and fail to generalize reliably Leng et al. (2024); Zhao et al. (2024). Moreover, they apply uniform weighting across all visual features, offering no mechanism to selectively adjust bias at the level of individual featuresZhang et al. (2024b); Manevich & Tsarfaty (2024). This coarse treatment limits their effectiveness in mitigating co-occurrence bias, which arises from spurious statistical correlations between objects that are often represented by distinct visual features.

In this work, we propose an inference-based method that simultaneously addresses both text–visual bias and co-occurrence bias, without relying on auxiliary models or external supervision. The core of our approach is the estimation of underlying bias, achieved by quantifying the contribution of individual tokens—both visual features and text tokens—through gradients derived from a first-order Taylor expansion. Building on this analysis, the method mitigates hallucinations by reweighting tokens via two key components: (1) suppressing the influence of visual features that exhibit strong spurious correlations with the current output token, thereby reducing co-occurrence bias; and (2) rebalancing cross-modal contributions by enhancing the role of visual features to align more closely with that of text tokens in generating the current output. As illustrated in Fig. 1, our method, GACD, corrects hallucinated predictions—such as the spurious generation of "beer" in the presence of "fork" and "spoon"—by amplifying the contributions of visual tokens unrelated to those nouns, leading to outputs that are more faithfully grounded in the visual modality. Note also that our method is readily applicable to existing MLLMs at inference time.

We summarize our main contributions as follows.

- We introduce an inference-based method for hallucination mitigation in MLLMs, built on a principled estimation of underlying bias via gradients obtained from a first-order Taylor expansion. This estimation provides a mechanism for understanding and granularly adjusting their influences of individual visual features and text tokens on the generation of the current output token, all without requiring auxiliary models or finetuning.
- We design two complementary modules: (i) suppression of spurious visual features correlated with the current output token to alleviate co-occurrence bias, and (ii) cross-modal rebalancing to enhance the contributions of visual features relative to text tokens, thereby addressing text–visual bias.
- Extensive experiments demonstrate that GACD mitigates hallucinations and enhances accuracy without sacrificing information. GACD achieves up to 8% increase in overall score on AMBER Wang et al. (2023), an 8% F1 boost on POPE Li et al. (2023b), up to 45% improvement in detailness and a 92% accuracy gain on LLaVA-QA90 Liu et al. (2024b).

2 Related Work

Hallucination and Bias. Hallucinations in LLMs often arise from biases in the training data McKenna et al. (2023); Huang et al. (2025), while in MLLMs, studies Tonmoy et al. (2024); Li et al. (2023b); Fu et al. (2024) show that hallucinations are closely linked to biases like text-visual and co-occurrence biases. Additionally, biases related to output position, which increase the risk of hallucination as output length grows, have been examined in Favero et al. (2024); Zhou et al. (2023b). Existing methods Li et al. (2023b); Fu et al. (2024); Kim et al. (2024) typically report only overall statistics, lacking a mathematical, sample-wise bias measurement. This distinction is impor-

tant, as biases can vary case by case. Our approach measures sample-dependent bias via token-level gradient sensitivities, revealing how pre-trained MLLM parameters embed these biases Kim et al. (2019); Guo et al. (2024), and enabling self-reflective hallucination mitigation.

Hallucination Mitigation. Training-related hallucination mitigation methods Chen et al. (2023a); Jiang et al. (2024); Yue et al. (2024); Peng et al. (2025); Zadeh et al. (2025) are expensive, requiring access to training data and specialized statistical analysis. Among them, LPOI Zadeh et al. (2025) also employs an object-aware framework, highlighting the effectiveness of modeling object-level information for mitigating hallucinations. Reinforcement-learning approaches Xing et al. (2024); Deng et al. (2024); Zhai et al. (2024) rely on supplementary feedback, often from human annotators or auxiliary LLMs/MLLMs, and the latter may themselves hallucinate. By contrast, post-decoding techniques modify model logits at inference time without further training or external feedback, making them lightweight add-ons. In text-only LLMs, such methods aim to align outputs with factual knowledge Chuang et al. (2023); Li et al. (2023a). In MLLMs, post-decoding strategies emphasize the role of visual inputs Leng et al. (2024); Zhao et al. (2024); Favero et al. (2024) and can be classified into image-level and token-level interventions. Image-level decoding methods Zhang et al. (2024b); Manevich & Tsarfaty (2024) treat all objects in the input image uniformly, limiting their effectiveness in addressing co-occurrence hallucinations. Existing token-level methods either rely on external segmentation Chen et al. (2024a) and detection models Kan et al. (2024) or lack awareness of object-related decoupling Woo et al. (2024). Moreover, these methods typically introduce an implicit trade-off between accuracy and informativeness, reducing hallucinations at the expense of omitting valid details. Attention-based methods Tang et al. (2025); Zhang et al. (2024a) require careful selection of specific layers and often introduce model-specific adjustments or heuristics. In contrast, our GACD directly estimates embedded bias and decouples object-aware visual tokens, enabling sample-specific hallucination mitigation without external data, models, or model-specific adjustments, while achieving a more favorable balance between accuracy and informativeness.

3 METHOD

In this section, we provide background on MLLMs, introduce the concept of token influence, and explain how GACD balances token influence to mitigate hallucinations.

3.1 BACKGROUND ON MLLMS

MLLMs generate a finite token sequence $\mathbf{y} = [y_1, \ldots, y_M]$ in response to a visual input (image or video) and a textual prompt. Let $\mathcal{V}$ be a finite vocabulary. The prompt is tokenized as $\mathbf{t}^p = [t_1^p, \ldots, t_N^p]$ with $t_n^p \in \mathcal{V}$. The visual input is encoded by a visual encoder into features, which are then projected into the token-embedding space $\mathbb{R}^d$, yielding visual tokens $\mathbf{t}^v = [t_1^v, \ldots, t_S^v]$ with $t_s^v \in \mathbb{R}^d$, where d is the shared token embedding dimension used for $\mathcal{V}$.

A MLLM with parameters θ computes, at each decoding step m, a logit vector

$$\mathbf{z}_m \;=\; \pi_\theta(\mathbf{t}^v,\, \mathbf{t}^p,\, \mathbf{y}_{<m}) \in \mathbb{R}^{|\mathcal{V}|}, \qquad \mathbf{y}_{<m} = [y_1, \ldots, y_{m-1}] \text{ (empty when } m = 1). \tag{1}$$

This induces a categorical next-token distribution via the softmax $\sigma : \mathbb{R}^{|\mathcal{V}|} \to \Delta^{|\mathcal{V}|-1}$:

$$p_\theta(y_m \mid \mathbf{t}^v, \mathbf{t}^p, \mathbf{y}_{<m}) \;=\; \big[\sigma(\mathbf{z}_m)\big]_{y_m}, \qquad 1 \le m \le M, \tag{2}$$

where $\sigma(\mathbf{z}_m) \in \Delta^{|\mathcal{V}|-1}$ denotes the probability distribution[1] over the vocabulary, and $[\cdot]_{y_m}$ selects the component corresponding to token $y_m \in \mathcal{V}$. At inference, y_m is sampled from this categorical distribution (e.g., greedy, beam search). The sequence likelihood factorizes by the chain rule:

$$p_\theta(\mathbf{y} \mid \mathbf{t}^v, \mathbf{t}^p) \;=\; \prod_{m=1}^{M} p_\theta(y_m \mid \mathbf{t}^v, \mathbf{t}^p, \mathbf{y}_{<m})\,. \tag{3}$$

Given a dataset $\mathcal{D}$ of $(\mathbf{t}^v, \mathbf{t}^p, \mathbf{y})$, maximum-likelihood training (or fine-tuning) estimates $\theta^\star$ by maximizing the conditional log-likelihood. Pretrained MLLMs encode statistical regularities (including spurious correlations) from training data in $\theta^\star$; such behavior can be probed without changing $\theta^\star$ via parameter-dependent analyses (e.g., gradients/attributions or counterfactual decodings) Kim et al. (2019); Guo et al. (2024), enabling self-reflective bias interpretation.

[1] We use "confidence" to denote the model-assigned probability of the emitted token.

3.2 Gradient-Based Token Influence Estimation

To capture these embeded biases, we measure how each input token perturbs the output logits. Let $\mathbf{z}_m^\star \in \mathbb{R}^{|\mathcal{V}|}$ denote the step-m logits $\mathbf{z}_m^\star = \pi_{\theta^\star}(\mathbf{t}^v, \mathbf{t}^p, \mathbf{y}_{<m})$. Around a reference sample point $(\mathbf{t}^{v(0)}, \mathbf{t}^{p(0)}, \mathbf{y}_{<m}^{(0)})$, the first-order Taylor expansion Spivak (1980) of the logits $\mathbf{z}_m^\star$ is

$$\mathbf{z}_m^\star \approx \sum_{s=1}^{S} \mathbf{g}_{ms}^v t_s^v + \sum_{n=1}^{N} \mathbf{g}_{mn}^p t_n^p + \sum_{i=1}^{m-1} \mathbf{g}_{mi}^y y_i + Const, \tag{4}$$

where $Const$ denotes other terms that are constant w.r.t., $\mathbf{t}^v$ and $\mathbf{t}^p$ and the token-wise Jacobians are

$$\mathbf{g}_{ms}^v := \frac{\partial \mathbf{z}_m^\star}{\partial \mathbf{t}_s^v}\Big|_{\mathbf{t}^v=\mathbf{t}^{v(0)}}, \qquad \mathbf{g}_{mn}^p := \frac{\partial \mathbf{z}_m^\star}{\partial \mathbf{t}_n^p}\Big|_{\mathbf{t}^p=\mathbf{t}^{p(0)}}, \qquad \mathbf{g}_{mi}^y := \frac{\partial \mathbf{z}_m^\star}{\partial \mathbf{y}_i}\Big|_{\mathbf{y}=\mathbf{y}_{<m}^{(0)}}, \tag{5}$$

where $\big|_{\cdot}$ indicate evaluation at the reference sample point. Taylor expansion details are in supplementary Sec. A. Each $\mathbf{g}_{ms}^v$, $\mathbf{g}_{mn}^p$, $\mathbf{g}_{mi}^y$ indicate a small token perturbation in its corresponding embedding space to a perturbation of the predict logit vector in $\mathbb{R}^{|\mathcal{V}|}$. We score the importance of each input token by the Manhattan norm of its gradient:

$$I_{ms}^v = \|\mathbf{g}_{ms}^v\|_1, \qquad I_{mn}^p = \|\mathbf{g}_{mn}^p\|_1, \qquad I_{mi}^y = \|\mathbf{g}_{mi}^y\|_1, \tag{6}$$

and $I_{ms}^v[c]$ represents the gradient from the output vocabulary c with respect to each visual tokens. Aggregating over tokens yields step-m group-level influences:

$$\mathtt{I}_m^v = \sum_{s=1}^{S} I_{ms}^v, \qquad \mathtt{I}_m^p = \sum_{n=1}^{N} I_{mn}^p, \qquad \mathtt{I}_m^y = \sum_{i=1}^{m-1} I_{mi}^y. \tag{7}$$

These quantities decompose, at the sample level, how visual tokens, prompt tokens, and prior outputs contribute to the logit of y_m, enabling interpretation of bias per sample.

3.3 Influence-Aware Constrained Decoding

GACD builds on token influence estimation with two components: (i) Object-aware Visual Token Grouping and (ii) Anchor-specific Influence-weighted Decoding. At step m, the former partitions visual tokens into object-related $\mathbf{t}^o$ and unrelated $\mathbf{t}^u$ based on objects detected in $\mathbf{y}_{<m}$. The latter extends contrastive decoding Li et al. (2022) by forming *Anchor-specific* negative guidance logits from pre-mentioned objects and computing a decoding weight α_m from token-influence measurements.

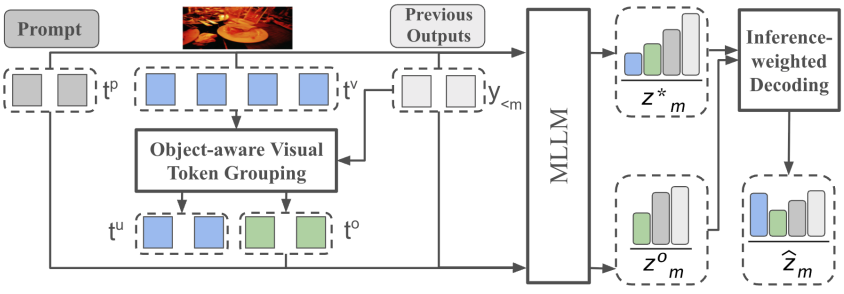

Figure 2: Overview of GACD. The method comprises (i) Object-aware Visual Token Grouping and (ii) Anchor-specific Influence-Weighted Decoding. At step m, previously mentioned objects are detected from $\mathbf{y}_{<m}$; visual tokens are partitioned into object-related textcolordarkgreen$\mathbf{t}^o$ and unrelated $\mathbf{t}^u$ via token influence (Sec. 3.2). Anchor-specific Influence-weighted Decoding extends contrastive decoding with token influence, explicitly amplifying the influence of $\mathbf{t}^u$ to jointly counter text-visual and co-occurrence biases; negative-guidance logits $\mathbf{z}_m^o$ are generated from $\{\mathbf{t}^o, \mathbf{t}^p, \mathbf{y}_{<m}\}$ to suppress text tokens and anchor-specific visual cues. Grouping is invoked only for noun prediction (where co-occurrence arises between object pairs); for non-noun prediction, we set $\mathbf{t}^o = \varnothing$ and uniformly amplify all visual tokens to balance text–visual bias.

Object-aware Visual Token Grouping. For each step m, we detect nouns in $\mathbf{y}_{<m}$ and treat each noun y_i as an object mention. To link a mention to visual evidence, we measure the influence I^v_{is} of visual token s on step i, For every noun y_i, the visual token with maximal influence is selected to form a mask $\mathcal{M}_{is}$. The cumulative object mask at step m aggregates all prior noun-linked tokens:

$$\mathcal{M}_{ms} = \mathbf{1}\left[\sum_{i=1}^{m-1} \mathcal{M}_{is} > 0\right], \quad \mathcal{M}_{is} = \mathbf{1}\left[y_i \in \text{Noun} \ \wedge \ s = \arg\max_j I^v_{ij}\right], \tag{8}$$

where $\mathbf{1}[\cdot]$ is the indicator and $\wedge$ is logical AND.

The mask $\mathcal{M}_{ms}$ identifies visual tokens linked to nouns emitted before m. We then partition the visual tokens into *object-related (*$\mathbf{t}^o$*)* and *unrelated-to-objects (*$\mathbf{t}^u$*)* sets via a Hadamard product:

$$\mathbf{t}^o \ = \ \mathbf{t}^v \odot \mathcal{M}_m, \qquad \mathbf{t}^u \ = \ \mathbf{t}^v \odot (\mathbf{1} - \mathcal{M}_m). \tag{9}$$

Object-related and unrelated influences at step m are

$$\mathtt{I}^o_m \ = \ \sum_{s=1}^{S} \|\mathbf{g}^v_{ms}\|_1 \, \mathcal{M}_{ms}, \qquad \mathtt{I}^u_m \ = \ \sum_{s=1}^{S} \|\mathbf{g}^v_{ms}\|_1 \, (1 - \mathcal{M}_{ms}). \tag{10}$$

Masking and grouping are applied only during noun prediction (mitigate co-occurrence hallucination from object pairs). For non-noun steps, all elements in $\mathcal{M}_m$ are set to 0, yielding an empty $\mathbf{t}^o$.

Anchor-specific Influence-weighted Decoding. Let $\mathbf{z}^o_m = \pi_{\theta^\star}(\mathbf{t}^o, \mathbf{t}^p, \mathbf{y}_{<m})$ the *anchor-specific* negative logits and $\mathbf{z}^\star_m = \pi_{\theta^\star}(\mathbf{t}^v, \mathbf{t}^p, \mathbf{y}_{<m})$ be the *original* logits. We adjust logits by

$$\hat{\mathbf{z}}_m \ = \ (1 + \alpha_m)\, \mathbf{z}^\star_m \ - \ \alpha_m \, \mathbf{z}^o_m, \tag{11}$$

with $\alpha_m \ \geq \ 0$. In the probability space, moving along $\mathbf{z}^\star_m - \mathbf{z}^o_m$ increases the KL divergence $D_{\mathrm{KL}}(\sigma(\mathbf{z}^\star_m) \| \sigma(\mathbf{z}^o_m))$ (see Sec. B). The original logits distribution $\mathbf{z}^\star_m$ can be viewed as $\pi_{\theta^*}(\mathbf{t}^u, \mathbf{t}^o, \mathbf{t}^p, \mathbf{y}_{<m})$, i.e., a joint distribution that additionally depends on $\mathbf{t}^u$ compare to $\mathbf{z}^o_m$. Increasing the KL divergence therefore emphasizes the contribution of tokens $\mathbf{t}^u$, which are unrelated to previous mentioned objects, thereby mitigating co-occurrence bias in noun prediction. For non-noun steps, $\mathbf{t}^u$ coincides with $\mathbf{t}^v$, meaning that all visual tokens are emphasized. This adjustment helps reduce text–visual hallucination.

When analyzing token influence of $\hat{\mathbf{z}}_m$ in Eq. 11, the chain rule shows that $\mathbf{t}^u$ occur only in the original logits $\mathbf{z}^\star_m$ and are amplified by $(1 + \alpha_m)$, whereas other inputs also contribute to $\mathbf{z}^o_m$ and therefore undergo smaller influence changes. Let $\tilde{\mathtt{I}}^o_m, \tilde{\mathtt{I}}^p_m, \tilde{\mathtt{I}}^y_m$ denote group influences computed on the negative branch $\mathbf{z}^o_m$ (analogous to equation 7). We then choose α_m so that the influence of $\mathbf{t}^u$ matches the *dominant text* level, $\mathtt{I}^t_m := \max(\mathtt{I}^p_m, \mathtt{I}^y_m)$. Aligning $\mathbf{t}^u$ influence with the question prompt $\mathtt{I}^p_m$ is crucial for visually grounded responses, while balancing with previous outputs $\mathtt{I}^y_m$ prevents visual forgetting.

$$\alpha_m = \frac{\mathtt{I}^t_m - \mathtt{I}^v_m}{\mathtt{I}^v_m - \tilde{\mathtt{I}}^o_m + \tilde{\mathtt{I}}^t_m - \mathtt{I}^t_m}, \tilde{\mathtt{I}}^t_m = \begin{cases} \tilde{\mathtt{I}}^p_m & \text{if } \mathtt{I}^p_m \geq \mathtt{I}^y_m \\ \tilde{\mathtt{I}}^y_m & \text{otherwise} \end{cases} \tag{12}$$

Unlike existing decoding methods Zhou et al. (2023b); Favero et al. (2024); Leng et al. (2024), which rely on adaptive plausibility constraints (e.g., prediction confidence) and require experimental tuning to determine optimal thresholds, our approach explicitly enforces non-negativity on the influence of object-related visual and prompt tokens. This corresponds to the following upper-bound condition:

$$0 \ \leq \ \alpha_m \ \leq \ \min\left\{ \frac{\mathtt{I}^o_m}{\tilde{\mathtt{I}}^o_m - \mathtt{I}^o_m}, \ \frac{\mathtt{I}^p_m}{\tilde{\mathtt{I}}^p_m - \mathtt{I}^p_m} \right\}. \tag{13}$$

Sample-dependent early stopping. Additionally, since hallucinations are more likely in long generations Zhou et al. (2023b); Peng et al. (2025), we introduce a sample-dependent stopping criterion based on visual influence. Specifically, if the visual influence ratio r^v_m of the token following the end-of-sequence (EOS) falls below a threshold ϵ,

$$r^v_m \ := \ \frac{\mathtt{I}^v_m}{\mathtt{I}^v_m + \mathtt{I}^p_m + \mathtt{I}^y_m} \ < \ \epsilon \quad \text{and} \quad y_{m-1} = \text{EOS}. \tag{14}$$

Early stopping is triggered to prevent further output generation with minimal visual grounding.

4 EXPERIMENTS

The proposed method is evaluated for both the open-ended generative tasks and the discriminative tasks. We use Amber Wang et al. (2023), MSCOCO Lin et al. (2014) and LLaVa-QA90 Liu et al. (2024b) datasets for the generative task, and Amber Wang et al. (2023) and POPE Li et al. (2023b) datasets on the discriminative tasks.

Evaluation Metrics. For generative image captioning, we focus on object hallucination and follow Deng et al. (2024) report the Caption Hallucination Assessment with Image Relevance (CHAIR) Rohrbach et al. (2018) score, which includes sentence-level (hal,C_S) and instance-level (cha,C_I) percentages, instance-level recall (R,cov), and the average generated length (Len) [2], as well as co-occurrence object hallucination (cog) and the overall $score$ as suggested by Wang et al. (2023). For generative VQA, follow Leng et al. (2024); Huang et al. (2024) GPT-4V Achiam et al. (2023) is used to score both accuracy (Acc) and detailedness (Det) on a scale of 10. For discriminative tasks, hallucination manifests as a 'yes/no' misclassification we report both accuracy and F1 score.

Implementation Details. The maximum output length is set to 256 across all models, with other model parameters kept at their defaults. To prevent excessive modifications, we set the maximum amplification factor, α_m, to 5 for discriminative tasks and 3 for generative tasks. We empirically set the early stopping thresholds ϵ as follows: LLaVA-v1.5 and LLaVA-v1.6: 7%, InstrucBLIP: 25%, mPLUG-Owl2: 2.5%, and InternVL2: 10%. All experiments are performed on an NVIDIA A40 GPU with batch size of 1. Unless otherwise specified, we use greedy sampling Graves (2013).

4.1 RESULTS ON OPEN-ENDED GENERATION

In this section, we compare against SOTA alignment-based method RLAIF-V and contrastive decoding methods VCD, M3ID, and AVISC, on the AMBER and MSCOCO datasets, as presented in Tab. 1, Tab. 2. Additionally, we evaluate our method against VCD on the LLaVA-QA90 dataset, presented in Tab. 3. Our method outperforms most existing approaches across various baseline models and datasets, highlighting its robustness and reliable performance across different data types and model architectures. Specifically, we surpass image-level contrastive decoding methods like VCD and M3ID, demonstrating its effectiveness in operating at the token level and adapting to individual samples. Furthermore, compared to the token-level AVISC, our method excels, likely due to its object awareness and adaptability to fluctuating bias levels. The results further demonstrate that our method effectively mitigates hallucinations while preserving information.

Table 1: Results on the AMBER Dataset.

MLLMs	Method	Generative				Discriminative				Score ↑
		cha ↓	cov ↑	hal ↓	cog ↓	acc ↑	P ↑	R ↑	F1 ↑	
LLaVA v1.5	base	7.8	**51.0**	36.4	4.2	72.0	**93.2**	62.4	74.7	83.5
	RLAIF-V 51	6.6	49.7	32.0	2.9	76.7	92.0	78.1	84.5	89.0
	VCD 26	6.7	46.4	32.6	3.5	71.3	91.1	62.3	74.3	83.8
	M3ID 12	6.2	50.5	29.3	2.8	72.4	91.8	64.1	75.5	84.7
	AVISC 48	6.5	50.2	34.8	2.7	73.8	89.7	68.4	77.6	85.5
	Ours	**5.6**	**51.0**	**24.3**	**1.8**	**80.3**	82.9	**89.3**	**86.0**	**90.2**
Instruct BLIP	base	8.8	**52.2**	38.2	4.4	76.5	84.5	79.0	81.7	86.5
	RLAIF-V 51	7.6	47.7	29.9	2.8	76.5	84.5	79.0	81.7	87.1
	VCD 26	7.9	49.7	36.7	3.7	75.9	83.5	79.3	81.3	86.7
	M3ID 12	7.3	49.2	33.8	3.7	75.8	84.4	77.9	81.0	86.9
	AVISC 48	7.1	48.8	34.4	4.3	75.9	83.4	**79.5**	81.4	87.2
	Ours	**6.0**	49.4	**26.6**	**2.4**	**78.1**	**88.8**	76.6	**82.2**	**88.1**
mPLUG Owl2	base	10.6	52.0	39.9	4.5	75.6	**95.0**	66.9	78.5	84.0
	RLAIF-V 51	7.8	50.5	35.7	4.1	81.2	90.8	79.7	84.9	88.6
	VCD 26	8.0	51.3	35.3	4.1	75.6	83.5	78.8	81.1	86.6
	M3ID 12	7.8	51.7	34.9	4.1	75.9	83.5	79.3	81.3	86.8
	AVISC 48	10.9	50.5	35.5	4.4	82.1	90.7	81.4	85.8	87.5
	Ours	**7.5**	**53.6**	**34.7**	**4.0**	**82.1**	87.0	**86.2**	**86.6**	**89.6**

Hallucination Mitigation. Our approach reduces hallucination by up to 33% at sentence-level (hal in Tab. 1 and C_S in Tab. 2) and 32% at instance-level (cha in Tab. 1 and C_I in Tab. 2), demonstrating its effectiveness in mitigating overall hallucinations. It also effectively mitigates co-occurrence hallucinations, with reductions of up to 57% for cog in Tab. 1. Accuracy gains of up to 92% (Tab. 3)

[2] Since shorter outputs can trivially lower CHAIR scores at the expense of informativeness.

Table 2: Results Using the CHAIR Metric on the MSCOCO Subset Following Deng et al. (2024).

Method	LLaVA-v1.5				InstructBLIP				mPLUG-Owl2			
	$C_S \downarrow$	$C_I \downarrow$	$R \uparrow$	$Len \uparrow$	$C_S \downarrow$	$C_I \downarrow$	$R \uparrow$	$Len \uparrow$	$C_S \downarrow$	$C_I \downarrow$	$R \uparrow$	$Len \uparrow$
base	48.8	13.4	**78.6**	99.8	57.8	16.5	**73.6**	101.3	59.2	17.6	**75.8**	105.3
VCD	44.8	12.8	76.8	89.8	63.4	19.6	71.2	95.5	52.7	16.1	73.2	93.6
M3ID	44.5	12.1	77.0	85.1	57.3	16.1	72.5	100.1	52.4	15.8	72.7	92.6
AVISC	46.4	13.4	76.3	90.5	58.9	17.8	70.6	99.6	58.3	17.5	75.6	99.5
Ours	**41.0**	**10.9**	77.3	85.0	**47.4**	**13.4**	72.3	93.9	**45.0**	**12.4**	74.9	83.5

further demonstrate that our model improves alignment with the input image, highlighting its ability to jointly address text–visual and co-occurrence biases (Sec. 4.4).

Information Preservation. Our method also enhances information preservation, with recall (cov in Tab. 1 and R in Tab. 2) dropping by an average of only 1.1%, compared to an average drop of 3.2% in other methods, and even increasing by 3.1% when using the baseline mPLUG-Owl2 on the AMBER dataset. Higher recall indicates that our model retrieves a broader range of objects from visual inputs. Additionally, results in Tab. 3 an increase of up to 45% in detailedness (Det), further demonstrating our method's effectiveness in retrieving all relevant visual details and mitigating visual forgetting.

4.2 Results on Discriminative Task

We next evaluate our method on discriminative tasks using AMBER (discriminative VQA) and POPE (existence VQA), with results shown in Tab. 1 and Tab. 4. Our approach achieves a better balance between precision and recall, yielding consistently higher F1 scores and improved accuracy. Notably, unlike competing methods that degrade Intern-VL2, ours preserves its performance via bias awareness, though improvements differ across categories and MLLMs.

Table 3: Results on LLaVA-QA90 Dataset, with All Settings Following Leng et al. (2024).

Method	LLaVA-v1.5		IntructBLIP		mPLUG-Owl2	
	Acc↑	Det↑	Acc↑	Det↑	Acc↑	Det↑
base	3.23	3.54	3.84	4.07	4.07	4.33
VCD	4.15	3.85	4.23	4.69	4.52	4.64
Ours	**6.20**	**5.13**	**6.28**	**4.77**	**6.69**	**6.28**

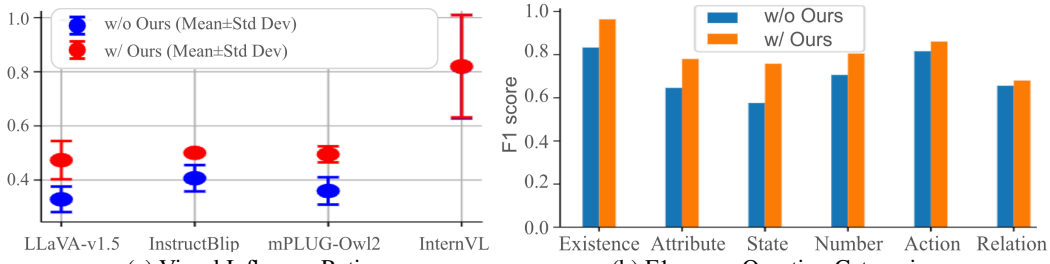

(a) Visual Influence Ratio (b) F1 across Question Categories

Figure 3: (a) Visual influence ratios across the POPE dataset, illustrating variation across MLLMs. Our method successfully increases the visual influence ratio when it falls below 50%. (b) F1 scores for the AMBER discriminative task using LLaVA-v1.5 are consistently improved by our method, with particularly notable gains in the existence and state categories.

Variation in Improvement Across Question Categories. Fig. 3b presents F1 scores across various question categories using LLaVA-v1.5 Liu et al. (2024a). Our method improves performance across all categories, with the largest gains in existence, attributes, and state—categories strongly tied to visual cues, benefiting from enhanced visual token influence.

Table 4: Results on POPE in MSCOCO Adversarial Setting.

Method	LLaVA-v1.5		InstructBLIP		mPLUG-Owl2		InternVL2	
	Acc↑	F1↑	Acc↑	F1↑	Acc↑	F1↑	Acc↑	F1↑
base	79.4	81.6	79.8	81.4	72.5	77.5	**85.8**	**85.0**
VCD	80.9	81.3	79.6	79.5	74.2	78.8	83.2	82.2
M3ID	81.7	81.8	81.0	81.6	75.6	79.1	83.5	82.1
AVISC	81.2	81.6	81.8	81.9	80.9	79.7	85.3	84.6
Woodpecker	80.5	80.6	79.0	78.6	77.5	76.9	85.7	84.8
Ours	**83.5**	**82.1**	**82.5**	**82.1**	**84.2**	**83.7**	**85.8**	**85.0**

Variation in Improvement Across MLLMs. Our method achieves the most significant improvement on mPLUG-Owl2 in object existence VQA (Tab. 4) and on LLaVA-v1.5 across various VQA categories (Tab. 1 discriminative), with minor improvement observed on InternVL2. This variation in performance correlates with the baseline visual influence ratios of the MLLMs. Fig. 3a presents the visual influence ratios in object existence VQA, showing that LLaVA-v1.5 exhibits the lowest visual contribution, followed by mPLUG-Owl2. This lower baseline visual influence ratio allows

our method to make more impactful adjustments. In contrast, InternVL2 has an original visual influence ratio exceeding 50%, resulting in minimal improvement when our method is applied. The strong performance of InternVL2 can be attributed to its original high visual influence ratio, further validating the motivation behind our approach. However, this dominant visual influence ratio in InternVL2 is not consistent across other question categories or in open-ended generation tasks [3], which allows our method to enhance its performance on the AMBER dataset (Tab. 6).

4.3 Results on Additional MLLMs and Datasets

We further evaluate modern MLLMs, LLaVA-v1.6, Qwen2-VL and Intern-VL2, on the Amber dataset. As shown in Tab. 6 (supplementary), our method consistently improves performance, even for strong baselines. To test generality, we also evaluate on MMBench Liu et al. (2025), MMVet Yu et al. (2023), ScienceQA Lu et al. (2022), and VizWiz Gurari et al. (2018). Results (supplementary) show that our approach enhances perception and recognition, especially for tasks with clear visual grounding, while preserving overall task performance and demonstrating robustness.

4.4 Ablation Study

In this section, we first analyze text–visual and co-occurrence biases, and then study the contributions of our proposed components. Further details on gradient computation methods, norm selection, and hyperparameter settings are provided in the supplementary material.

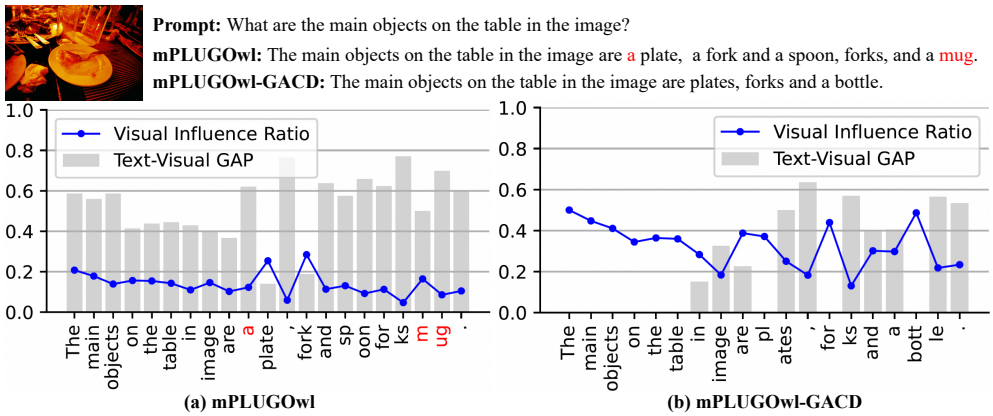

(a) mPLUGOwl **(b) mPLUGOwl-GACD**

Figure 4: Comparison of visual influence ratios r_m^v and Text-Visual GAP, with and without our GACD. (a) Without GACD, mPLUG-Owl2 shows a low initial visual influence ratio, punctuation marks and suffixes naturally have low visual influence, while objects start with higher influence that declines as the sequence grows. Hallucinations tend to occur when the visual ratio is low. The text-visual gap confirms that text dominates the influence on predictions. (b) With GACD, the visual influence ratio increases overall and mitigates the decrease over the sequence length. The text tokens only domain influence in predictions less related to the visual, reducing hallucination.

Text-Visual Bias Analysis. Fig. 3a shows that with the exception of InternVL2, MLLMs – LLaVA-v1.5, InstructBLIP, and mPLUG-Owl2 – rely more on text prompt than on visual input. Likely due to MLLMs' training process, this tendency is common in MLLMs, where multimodal features are aligned with language tokens after extensive text-based pre-training, causing language components to dominate decision-making. GACD effectively increases overall visual influence to match that of object-present question prompts in POPE (Fig. 3a). In the open-ended generation task, we further observe the visual influence ratio r_m^v and the Text-Visual GAP, defined as $\max(\max(r_m^p, r_m^y) - r_m^v, 0)$, the difference between the text influence ratio and the visual influence ratio when text influence is dominant [4]. Observations in Fig. 4 also highlight the text-dominant influence typical of MLLMs. GACD counteracts this by boosting the influence of visual tokens when aligning them with prompts and previous outputs, leading to higher prediction confidence and a reduction in hallucinations (see Fig. 6 in supplementary). Additionally, the nature of the output token affects the degree of visual influence ratio. For instance, punctuation marks or suffixes tend to

[3] Results for other question categories and visualizations of open-ended generation are in supplementary.

[4] r_m^p and r_m^y are derived in the same manner as r_m^v in equation 14.

have a lower visual influence ratio. This is intuitive, as these tokens rely more on linguistic context and are less dependent on visual information. This observation highlights the value of our GACD framework delivering sample-dependent, token-specific hallucination mitigation.

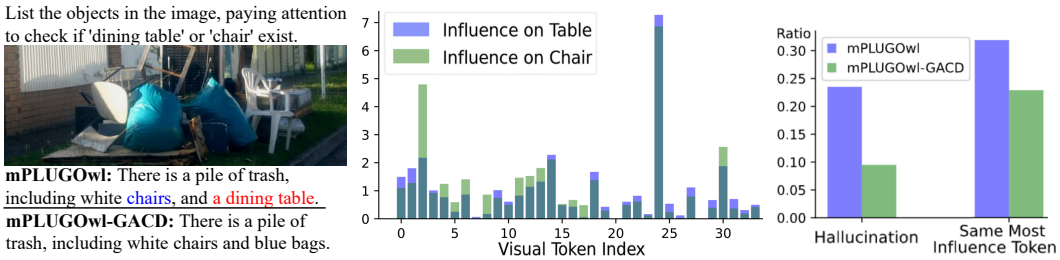

(a) Co-occurrence Hallucination (b) Individual Visual Token Influence (c) Overall Statistics

Figure 5: Co-occurrence hallucination of 'table' in the presence of 'chair'. (a) Comparison of outputs with and without GACD. (b) Visualization of individual visual token influence indicates that the visual token with index 24, which has the highest influence on the hallucinated 'table', also holds the highest influence on 'chair'. (c) Summary statistics for 100 chair-only and 100 table-only images, showing the hallucination rate and the percentage of cases where both objects share the same most influential visual token (as illustrated in b). GACD effectively reduces both metrics.

Co-occurrence Bias Analysis. Fig. 5a shows an example where mPLUG-Owl2 incorrectly predicts 'dining table' due to the presence of a 'chair'. In Fig. 5b, the influence of individual visual tokens on hallucinated prediction I_{ms}('table') and I_{ms}('chair') shows that they share the same most influential visual token: $s = 24$. We further collected 100 chair-only and 100 table-only images from MSCOCO evaluation dataset Lin et al. (2014). Results in Fig. 5c indicate that when only 'chair' or 'table' exists in the image, the hallucination rate for the other object is 23.5%, with a 31.9% rate of sharing the same most influential token. This indicates that the 'Same Most Influential Token' phenomenon is common in co-occurrence hallucinations. Our GACD effectively reduces the hallucination where both 'table' or 'chair' are predicted in single-object images.

Component Analysis. To assess the effectiveness of each component in our proposed method, we conducted the following variants: 1) Visual Amplification (VA) only: visual amplification is applied to all visual tokens ($\mathbf{t}^v$), including during noun predictions. 2) Co-occurrence Hallucination Reduction (CR): object-related visual tokens are detected, and $\mathbf{t}^u$ is amplified during noun predictions. 3) Our full model, with early stopping (ES). Tab. 5 demonstrates that each component of our method contributes to the overall performance. VA significantly reduces hallucinations while improving object recall. CR further mitigates co-occurrence bias, a residual form of the text-visual bias addressed by VA, resulting in additional hallucination reduction. Both VA and CR achieve these gains without introducing trade-offs. When necessary, the ES mechanism shortens outputs to effectively reduce hallucinations, with only a slight recall trade-off that remains acceptable for most MLLMs.

Table 5: Component Analysis Using the CHAIR Metric.

Components			LLaVA-v1.5				InstructBLIP				mPLUG-Owl2			
VA	CR	ES	$C_S \downarrow$	$C_I \downarrow$	$R \uparrow$	$Len \uparrow$	$C_S \downarrow$	$C_I \downarrow$	$R \uparrow$	$Len \uparrow$	$C_S \downarrow$	$C_I \downarrow$	$R \uparrow$	$Len \uparrow$
			48.8	13.4	78.6	99.8	57.8	16.5	73.6	101.3	59.2	17.6	75.8	105.3
✓			46.4	11.6	79.0	95.6	53.6	15.1	**75.3**	108.4	52.6	14.4	**78.2**	95.6
✓	✓		46.2	11.3	**79.4**	95.5	53.2	14.0	74.6	105.7	52.3	14.2	78.0	95.5
✓	✓	✓	**41.0**	**10.9**	77.3	85.0	**47.4**	**13.4**	72.3	93.9	**45.0**	**12.4**	74.9	83.5

5 Conclusion

In conclusion, we introduce a gradient-based self-reflection method to estimate token influence and quantitatively estimate bias severity. This estimation enables the identification of object-related visual tokens, which are then integrated into an influence-aware constrained decoding framework. This framework effectively mitigates both text-visual and co-occurrence biases, reducing hallucinations. Our method operates without requiring additional resources such as costly fine-tuning, extra models, or data statistics. Furthermore, to reduce text-visual bias in long-generated sequences, we propose a sample-dependent stopping criterion based on the proposed visual influence.

REFERENCES

Josh Achiam, Steven Adler, Sandhini Agarwal, Lama Ahmad, Ilge Akkaya, Florencia Leoni Aleman, Diogo Almeida, Janko Altenschmidt, Sam Altman, Shyamal Anadkat, et al. Gpt-4 technical report. *arXiv preprint arXiv:2303.08774*, 2023.

Jinze Bai, Shuai Bai, Shusheng Yang, Shijie Wang, Sinan Tan, Peng Wang, Junyang Lin, Chang Zhou, and Jingren Zhou. Qwen-vl: A frontier large vision-language model with versatile abilities. *arXiv preprint arXiv:2308.12966*, 2023.

Assaf Ben-Kish, Moran Yanuka, Morris Alper, Raja Giryes, and Hadar Averbuch-Elor. Mocha: Multi-objective reinforcement mitigating caption hallucinations. *arXiv preprint arXiv:2312.03631*, 2023.

Jun Chen, Deyao Zhu, Xiaoqian Shen, Xiang Li, Zechun Liu, Pengchuan Zhang, Raghuraman Krishnamoorthi, Vikas Chandra, Yunyang Xiong, and Mohamed Elhoseiny. Minigpt-v2: large language model as a unified interface for vision-language multi-task learning. *arXiv preprint arXiv:2310.09478*, 2023a.

Zhaorun Chen, Zhuokai Zhao, Hongyin Luo, Huaxiu Yao, Bo Li, and Jiawei Zhou. Halc: Object hallucination reduction via adaptive focal-contrast decoding. *arXiv preprint arXiv:2403.00425*, 2024a.

Zhe Chen, Jiannan Wu, Wenhai Wang, Weijie Su, Guo Chen, Sen Xing, Muyan Zhong, Qinglong Zhang, Xizhou Zhu, Lewei Lu, et al. Internvl: Scaling up vision foundation models and aligning for generic visual-linguistic tasks. In *Proceedings of the IEEE/CVF Conference on Computer Vision and Pattern Recognition*, pp. 24185–24198, 2024b.

Zhiyang Chen, Yousong Zhu, Yufei Zhan, Zhaowen Li, Chaoyang Zhao, Jinqiao Wang, and Ming Tang. Mitigating hallucination in visual language models with visual supervision. *arXiv preprint arXiv:2311.16479*, 2023b.

Yung-Sung Chuang, Yujia Xie, Hongyin Luo, Yoon Kim, James Glass, and Pengcheng He. Dola: Decoding by contrasting layers improves factuality in large language models. *arXiv preprint arXiv:2309.03883*, 2023.

Wenliang Dai, Junnan Li, Dongxu Li, Anthony Meng Huat Tiong, Junqi Zhao, Weisheng Wang, Boyang Li, Pascale Fung, and Steven Hoi. Instructblip: Towards general-purpose vision-language models with instruction tuning, 2023. URL https://arxiv.org/abs/2305.06500.

Ailin Deng, Zhirui Chen, and Bryan Hooi. Seeing is believing: Mitigating hallucination in large vision-language models via clip-guided decoding. *arXiv preprint arXiv:2402.15300*, 2024.

Joseph Enguehard. Sequential integrated gradients: a simple but effective method for explaining language models. *arXiv preprint arXiv:2305.15853*, 2023.

Alessandro Favero, Luca Zancato, Matthew Trager, Siddharth Choudhary, Pramuditha Perera, Alessandro Achille, Ashwin Swaminathan, and Stefano Soatto. Multi-modal hallucination control by visual information grounding. *arXiv preprint arXiv:2403.14003*, 2024.

Chaoyou Fu, Peixian Chen, Yunhang Shen, Yulei Qin, Mengdan Zhang, Xu Lin, Jinrui Yang, Xiawu Zheng, Ke Li, Xing Sun, Yunsheng Wu, and Rongrong Ji. Mme: A comprehensive evaluation benchmark for multimodal large language models, 2024. URL https://arxiv.org/abs/2306.13394.

Alex Graves. Generating sequences with recurrent neural networks. *arXiv preprint arXiv:1308.0850*, 2013.

Yufei Guo, Muzhe Guo, Juntao Su, Zhou Yang, Mengqiu Zhu, Hongfei Li, Mengyang Qiu, and Shuo Shuo Liu. Bias in large language models: Origin, evaluation, and mitigation. *arXiv preprint arXiv:2411.10915*, 2024.

Danna Gurari, Qing Li, Abigale J Stangl, Anhong Guo, Chi Lin, Kristen Grauman, Jiebo Luo, and Jeffrey P Bigham. Vizwiz grand challenge: Answering visual questions from blind people. In *Proceedings of the IEEE conference on computer vision and pattern recognition*, pp. 3608–3617, 2018.

Lei Huang, Weijiang Yu, Weitao Ma, Weihong Zhong, Zhangyin Feng, Haotian Wang, Qianglong Chen, Weihua Peng, Xiaocheng Feng, Bing Qin, et al. A survey on hallucination in large language models: Principles, taxonomy, challenges, and open questions. *ACM Transactions on Information Systems*, 43(2):1–55, 2025.

Qidong Huang, Xiaoyi Dong, Pan Zhang, Bin Wang, Conghui He, Jiaqi Wang, Dahua Lin, Weiming Zhang, and Nenghai Yu. Opera: Alleviating hallucination in multi-modal large language models via over-trust penalty and retrospection-allocation. In *Proceedings of the IEEE/CVF Conference on Computer Vision and Pattern Recognition*, pp. 13418–13427, 2024.

Chaoya Jiang, Haiyang Xu, Mengfan Dong, Jiaxing Chen, Wei Ye, Ming Yan, Qinghao Ye, Ji Zhang, Fei Huang, and Shikun Zhang. Hallucination augmented contrastive learning for multimodal large language model. In *Proceedings of the IEEE/CVF Conference on Computer Vision and Pattern Recognition*, pp. 27036–27046, 2024.

Zhangqi Jiang, Junkai Chen, Beier Zhu, Tingjin Luo, Yankun Shen, and Xu Yang. Devils in middle layers of large vision-language models: Interpreting, detecting and mitigating object hallucinations via attention lens. In *Proceedings of the Computer Vision and Pattern Recognition Conference*, pp. 25004–25014, 2025.

Zhehan Kan, Ce Zhang, Zihan Liao, Yapeng Tian, Wenming Yang, Junyuan Xiao, Xu Li, Dongmei Jiang, Yaowei Wang, and Qingmin Liao. Catch: Complementary adaptive token-level contrastive decoding to mitigate hallucinations in lvlms, 2024. URL https://arxiv.org/abs/2411.12713.

Cheongwoong Kang and Jaesik Choi. Impact of co-occurrence on factual knowledge of large language models. *arXiv preprint arXiv:2310.08256*, 2023.

Andrei Kapishnikov, Subhashini Venugopalan, Besim Avci, Ben Wedin, Michael Terry, and Tolga Bolukbasi. Guided integrated gradients: An adaptive path method for removing noise. In *Proceedings of the IEEE/CVF conference on computer vision and pattern recognition*, pp. 5050–5058, 2021.

Byungju Kim, Hyunwoo Kim, Kyungsu Kim, Sungjin Kim, and Junmo Kim. Learning not to learn: Training deep neural networks with biased data. In *Proceedings of the IEEE/CVF conference on computer vision and pattern recognition*, pp. 9012–9020, 2019.

Younghyun Kim, Sangwoo Mo, Minkyu Kim, Kyungmin Lee, Jaeho Lee, and Jinwoo Shin. Discovering and mitigating visual biases through keyword explanation. In *Proceedings of the IEEE/CVF Conference on Computer Vision and Pattern Recognition*, pp. 11082–11092, 2024.

Sicong Leng, Hang Zhang, Guanzheng Chen, Xin Li, Shijian Lu, Chunyan Miao, and Lidong Bing. Mitigating object hallucinations in large vision-language models through visual contrastive decoding. In *Proceedings of the IEEE/CVF Conference on Computer Vision and Pattern Recognition*, pp. 13872–13882, 2024.

Kenneth Li, Oam Patel, Fernanda Viégas, Hanspeter Pfister, and Martin Wattenberg. Inference-time intervention: Eliciting truthful answers from a language model. *Advances in Neural Information Processing Systems*, 36:41451–41530, 2023a.

Xiang Lisa Li, Ari Holtzman, Daniel Fried, Percy Liang, Jason Eisner, Tatsunori Hashimoto, Luke Zettlemoyer, and Mike Lewis. Contrastive decoding: Open-ended text generation as optimization. *arXiv preprint arXiv:2210.15097*, 2022.

Yifan Li, Yifan Du, Kun Zhou, Jinpeng Wang, Wayne Xin Zhao, and Ji-Rong Wen. Evaluating object hallucination in large vision-language models. *arXiv preprint arXiv:2305.10355*, 2023b.

Tsung-Yi Lin, Michael Maire, Serge Belongie, James Hays, Pietro Perona, Deva Ramanan, Piotr Dollár, and C Lawrence Zitnick. Microsoft coco: Common objects in context. In *Computer Vision–ECCV 2014: 13th European Conference, Zurich, Switzerland, September 6-12, 2014, Proceedings, Part V 13*, pp. 740–755. Springer, 2014.

Haotian Liu, Chunyuan Li, Yuheng Li, Bo Li, Yuanhan Zhang, Sheng Shen, and Yong Jae Lee. Llava-next: Improved reasoning, ocr, and world knowledge, 2024a.

Haotian Liu, Chunyuan Li, Qingyang Wu, and Yong Jae Lee. Visual instruction tuning. *Advances in neural information processing systems*, 36, 2024b.

Shi Liu, Kecheng Zheng, and Wei Chen. Paying more attention to image: A training-free method for alleviating hallucination in lvlms. In *European Conference on Computer Vision*, pp. 125–140. Springer, 2024c.

Yuan Liu, Haodong Duan, Yuanhan Zhang, Bo Li, Songyang Zhang, Wangbo Zhao, Yike Yuan, Jiaqi Wang, Conghui He, Ziwei Liu, et al. Mmbench: Is your multi-modal model an all-around player? In *European Conference on Computer Vision*, pp. 216–233. Springer, 2025.

Pan Lu, Swaroop Mishra, Tanglin Xia, Liang Qiu, Kai-Wei Chang, Song-Chun Zhu, Oyvind Tafjord, Peter Clark, and Ashwin Kalyan. Learn to explain: Multimodal reasoning via thought chains for science question answering. *Advances in Neural Information Processing Systems*, 35:2507–2521, 2022.

Daniel D Lundstrom, Tianjian Huang, and Meisam Razaviyayn. A rigorous study of integrated gradients method and extensions to internal neuron attributions. In *International Conference on Machine Learning*, pp. 14485–14508. PMLR, 2022.

Avshalom Manevich and Reut Tsarfaty. Mitigating hallucinations in large vision-language models (lvlms) via language-contrastive decoding (lcd), 2024. URL `https://arxiv.org/abs/2408.04664`.

Nick McKenna, Tianyi Li, Liang Cheng, Mohammad Javad Hosseini, Mark Johnson, and Mark Steedman. Sources of hallucination by large language models on inference tasks. *arXiv preprint arXiv:2305.14552*, 2023.

Yeji Park, Deokyeong Lee, Junsuk Choe, and Buru Chang. Convis: Contrastive decoding with hallucination visualization for mitigating hallucinations in multimodal large language models. *arXiv preprint arXiv:2408.13906*, 2024.

Shangpin Peng, Senqiao Yang, Li Jiang, and Zhuotao Tian. Mitigating object hallucinations via sentence-level early intervention. *arXiv preprint arXiv:2507.12455*, 2025.

Alec Radford, Jong Wook Kim, Chris Hallacy, Aditya Ramesh, Gabriel Goh, Sandhini Agarwal, Girish Sastry, Amanda Askell, Pamela Mishkin, Jack Clark, et al. Learning transferable visual models from natural language supervision. In *International conference on machine learning*, pp. 8748–8763. PMLR, 2021.

Anna Rohrbach, Lisa Anne Hendricks, Kaylee Burns, Trevor Darrell, and Kate Saenko. Object hallucination in image captioning. *arXiv preprint arXiv:1809.02156*, 2018.

Michael Spivak. Calculus. houston, tx: Publish or perish, 1980.

Zhiqing Sun, Sheng Shen, Shengcao Cao, Haotian Liu, Chunyuan Li, Yikang Shen, Chuang Gan, Liang-Yan Gui, Yu-Xiong Wang, Yiming Yang, et al. Aligning large multimodal models with factually augmented rlhf. *arXiv preprint arXiv:2309.14525*, 2023.

Feilong Tang, Zile Huang, Chengzhi Liu, Qiang Sun, Harry Yang, and Ser-Nam Lim. Intervening anchor token: Decoding strategy in alleviating hallucinations for mllms. In *The Thirteenth International Conference on Learning Representations*, 2025.

SM Tonmoy, SM Zaman, Vinija Jain, Anku Rani, Vipula Rawte, Aman Chadha, and Amitava Das. A comprehensive survey of hallucination mitigation techniques in large language models. *arXiv preprint arXiv:2401.01313*, 2024.

Junyang Wang, Yuhang Wang, Guohai Xu, Jing Zhang, Yukai Gu, Haitao Jia, Ming Yan, Ji Zhang, and Jitao Sang. An llm-free multi-dimensional benchmark for mllms hallucination evaluation. *arXiv preprint arXiv:2311.07397*, 2023.

Sangmin Woo, Donguk Kim, Jaehyuk Jang, Yubin Choi, and Changick Kim. Don't miss the forest for the trees: Attentional vision calibration for large vision language models. *arXiv preprint arXiv:2405.17820*, 2024.

Shangyu Xing, Fei Zhao, Zhen Wu, Tuo An, Weihao Chen, Chunhui Li, Jianbing Zhang, and Xinyu Dai. Efuf: Efficient fine-grained unlearning framework for mitigating hallucinations in multimodal large language models. *arXiv preprint arXiv:2402.09801*, 2024.

Qinghao Ye, Haiyang Xu, Jiabo Ye, Ming Yan, Anwen Hu, Haowei Liu, Qi Qian, Ji Zhang, and Fei Huang. mplug-owl2: Revolutionizing multi-modal large language model with modality collaboration. In *Proceedings of the IEEE/CVF Conference on Computer Vision and Pattern Recognition*, pp. 13040–13051, 2024.

Tianyu Yu, Haoye Zhang, Yuan Yao, Yunkai Dang, Da Chen, Xiaoman Lu, Ganqu Cui, Taiwen He, Zhiyuan Liu, Tat-Seng Chua, et al. Rlaif-v: Aligning mllms through open-source ai feedback for super gpt-4v trustworthiness. *arXiv preprint arXiv:2405.17220*, 2024.

Weihao Yu, Zhengyuan Yang, Linjie Li, Jianfeng Wang, Kevin Lin, Zicheng Liu, Xinchao Wang, and Lijuan Wang. Mm-vet: Evaluating large multimodal models for integrated capabilities. *arXiv preprint arXiv:2308.02490*, 2023.

Zihao Yue, Liang Zhang, and Qin Jin. Less is more: Mitigating multimodal hallucination from an eos decision perspective. *arXiv preprint arXiv:2402.14545*, 2024.

Fatemeh Pesaran Zadeh, Yoojin Oh, and Gunhee Kim. Lpoi: Listwise preference optimization for vision language models. *arXiv preprint arXiv:2505.21061*, 2025.

Bohan Zhai, Shijia Yang, Chenfeng Xu, Sheng Shen, Kurt Keutzer, Chunyuan Li, and Manling Li. Halle-control: Controlling object hallucination in large multimodal models, 2024. URL https://arxiv.org/abs/2310.01779.

Xiaofeng Zhang, Chen Shen, Xiaosong Yuan, Shaotian Yan, Liang Xie, Wenxiao Wang, Chaochen Gu, Hao Tang, and Jieping Ye. From redundancy to relevance: Enhancing explainability in multimodal large language models. *arXiv e-prints*, pp. arXiv–2406, 2024a.

Yi-Fan Zhang, Weichen Yu, Qingsong Wen, Xue Wang, Zhang Zhang, Liang Wang, Rong Jin, and Tieniu Tan. Debiasing large visual language models. *arXiv preprint arXiv:2403.05262*, 2024b.

Linxi Zhao, Yihe Deng, Weitong Zhang, and Quanquan Gu. Mitigating object hallucination in large vision-language models via classifier-free guidance. *arXiv preprint arXiv:2402.08680*, 2024.

Yibo Zhou, Hai-Miao Hu, Jinzuo Yu, Zhenbo Xu, Weiqing Lu, and Yuran Cao. A solution to co-occurrence bias: Attributes disentanglement via mutual information minimization for pedestrian attribute recognition. *arXiv preprint arXiv:2307.15252*, 2023a.

Yiyang Zhou, Chenhang Cui, Jaehong Yoon, Linjun Zhang, Zhun Deng, Chelsea Finn, Mohit Bansal, and Huaxiu Yao. Analyzing and mitigating object hallucination in large vision-language models. *arXiv preprint arXiv:2310.00754*, 2023b.

A First Order Taylor Expansion

Let $\mathbf{z}_m^\star \in \mathbb{R}^{|\mathcal{V}|}$ denote the step-m logits $\mathbf{z}_m^\star = \pi_{\theta^\star}(\mathbf{t}^v, \mathbf{t}^p, \mathbf{y}_{<m})$. Around a reference point $(\mathbf{t}^{v(0)}, \mathbf{t}^{p(0)}, \mathbf{y}_{<m}^{(0)})$, the detailed first-order Taylor expansion of the logit $\mathbf{z}_m^\star$ is

$$
\begin{aligned}
\mathbf{z}_m^\star \approx & \underbrace{\mathbf{z}_m^{\star(0)}}_{\pi_{\theta^\star}(\mathbf{t}^{v(0)}, \mathbf{t}^{p(0)}, \mathbf{y}_{<m}^{(0)})} + \sum_{s=1}^{S} \mathbf{g}_{ms}^v \Big(\mathbf{t}_s^v - \mathbf{t}_s^{v(0)}\Big) \\
& + \sum_{n=1}^{N} \mathbf{g}_{mn}^p \Big(\mathbf{t}_n^p - \mathbf{t}_n^{p(0)}\Big) + \sum_{i=1}^{m-1} \mathbf{g}_{mi}^y \Big(\mathbf{y}_i - \mathbf{y}_i^{(0)}\Big) \\
= & \sum_{s=1}^{S} \mathbf{g}_{ms}^v t_s^v + \sum_{n=1}^{N} \mathbf{g}_{mn}^p t_n^p + \sum_{i=1}^{m-1} \mathbf{g}_{mi}^y y_i \\
& + \underbrace{\mathbf{z}_m^{\star(0)} - \sum_{s=1}^{S} \mathbf{g}_{ms}^v t_s^{v(0)} - \sum_{n=1}^{N} \mathbf{g}_{mn}^p t_n^{p(0)} - \sum_{i=1}^{m-1} \mathbf{g}_{mi}^y y_i^{(0)}}_{Const}, \\
= & \sum_{s=1}^{S} \mathbf{g}_{ms}^v t_s^v + \sum_{n=1}^{N} \mathbf{g}_{mn}^p t_n^p + \sum_{i=1}^{m-1} \mathbf{g}_{mi}^y y_i + Const,
\end{aligned}
\tag{15}
$$

where the (token-wise) Jacobians are

$$
\mathbf{g}_{ms}^v \coloneqq \left.\frac{\partial \mathbf{z}_m^\star}{\partial \mathbf{t}_s^v}\right|_{\mathbf{t}^v = \mathbf{t}^{v(0)}}, \qquad \mathbf{g}_{mn}^p \coloneqq \left.\frac{\partial \mathbf{z}_m^\star}{\partial \mathbf{t}_n^p}\right|_{\mathbf{t}^p = \mathbf{t}^{p(0)}}, \qquad \mathbf{g}_{mi}^y \coloneqq \left.\frac{\partial \mathbf{z}_m^\star}{\partial \mathbf{y}_i}\right|_{\mathbf{y} = \mathbf{y}_{<m}^{(0)}}, \tag{16}
$$

and $\mathbf{z}_m^{\star(0)} = \pi_{\theta^\star}(\mathbf{t}^{v(0)}, \mathbf{t}^{p(0)}, \mathbf{y}_{<m}^{(0)})$. Here $\big|_{\cdot}$ denotes evaluation at the reference point. Each $\mathbf{g}_{ms}^v$, $\mathbf{g}_{mn}^p$, $\mathbf{g}_{mi}^y$ maps a small token perturbation in its corresponding embedding space to a perturbation of the logit vector in $\mathbb{R}^{|\mathcal{V}|}$. And $Const$ denotes all other terms that are constant w.r.t., the $\mathbf{t}^v, \mathbf{t}^p$.

B Interpreting Contrastive Decoding through KL Divergence

Kullback-Leibler (KL) divergence can be used to interpret contrastive decoding, It measures the divergence between the reference distribution $p_{\theta^\star}(y_{cm}|\mathbf{t}^o, \mathbf{t}^p, y_{<m})$ to the $\mathbf{t}^u$ joint distribution $p_{\theta^\star}(y_{cm}|\mathbf{t}^v, \mathbf{t}^p, y_{<m})$, where $\mathbf{t}^v = \{\mathbf{t}^u, \mathbf{t}^o\}$.

$$
\begin{aligned}
\mathrm{D}_{KL} &= \sum_c p_{\theta^\star}(y_{cm}|\mathbf{t}^v, \mathbf{t}^p, y_{<m}) \log\Big(\frac{p_{\theta^\star}(y_{cm}|\mathbf{t}^v, \mathbf{t}^p, y_{<m})}{p_{\theta^\star}(y_{cm}|\mathbf{t}^o, \mathbf{t}^p, y_{<m})}\Big) \\
&= \sum_c p_{\theta^\star}(y_{cm}|\mathbf{t}^v, \mathbf{t}^p, y_{<m}) \big(\log(p_{\theta^\star}(y_{cm}|\mathbf{t}^v, \mathbf{t}^p, y_{<m})) - \log(p_{\theta^\star}(y_{cm}|\mathbf{t}^o, \mathbf{t}^p, y_{<m}))\big) \\
&= \sum_c p_{\theta^\star}(y_{cm}|\mathbf{t}^v, \mathbf{t}^p, y_{<m}) \big([\pi_{\theta^*}(\mathbf{t}^v, \mathbf{t}^p)_m]_c - \log(\sum \exp(\pi_{\theta^*}(\mathbf{t}^v, \mathbf{t}^p)_m)) \\
&- [\pi_{\theta^*}(\mathbf{t}^o, \mathbf{t}^p)_m]_c + \log(\sum \exp(\pi_{\theta^*}(\mathbf{t}^o, \mathbf{t}^p)_m))\big) \\
&= \sum_c p_{\theta^\star}(y_{cm}|\mathbf{t}^v, \mathbf{t}^p, y_{<m}) \big(\underbrace{[\pi_{\theta^*}(\mathbf{t}^v, \mathbf{t}^p)_m - \pi_{\theta^*}(\mathbf{t}^o, \mathbf{t}^p)_m]_c}_{\text{adjustment term}} + Const\big),
\end{aligned}
\tag{17}
$$

where $p_{\theta^\star}(y_{cm}|\mathbf{t}^v, \mathbf{t}^p, y_{<m}) = \sigma(\pi_{\theta^*}(\mathbf{t}^v, \mathbf{t}^p)_m)$, $p_{\theta^\star}(y_{cm}|\mathbf{t}^o, \mathbf{t}^p, y_{<m}) = \sigma(\pi_{\theta^*}(\mathbf{t}^o, \mathbf{t}^p)_m)$ and c represents a class in the predefined vocabulary. The adjustment term increases the KL divergence, thereby emphasizing the impact of visual tokens.

C Result on modern MLLMs

We further evaluate recent MLLMs, LLaVA-v1.6, Qwen2-VL, and Intern-VL2, on the AMBER dataset. As shown in Tab. 6, our method consistently improves performance, even when the base

models already achieve strong results. Moreover, it surpasses SOTA comparison methods. This improvement stems from the model's self-reflection ability, which effectively identifies biases in baseline MLLMs and adapts the outputs accordingly.

Table 6: Latest MLLMs on the AMBER Dataset.

MLLMs	Method	Generative				Discriminative				Score ↑
		cha↓	cov↑	hal↓	cog↓	acc↑	P↑	R↑	F1↑	
LLaVA v1.6	base	9.9	56.7	47.4	4.3	80.3	82.9	**89.3**	86.0	88.5
	RLAIF-V	9.0	53.6	46.1	3.42	80.8	83.9	88.9	86.3	88.6
	VCD	9.5	52.7	46.3	3.78	79.9	83.1	87.6	85.4	88.0
	M3ID	9.2	50.1	45.3	3.3	80.4	83.2	88.8	85.9	88.4
	AVISC	9.2	50.7	47.5	3.2	80.6	83.5	88.2	85.8	88.3
	Ours	**8.7**	**58.3**	**43.8**	**2.5**	**81.2**	**85.2**	88.8	**87.0**	**89.2**
Qwen2 VL	base	6.4	70.4	54.8	5.9	82.9	**91.6**	82.2	86.6	90.1
	RLAIF-V	5.8	69.4	54.1	5.5	83.5	91.2	82.6	86.7	90.4
	VCD	6.5	69.1	53.7	5.3	82.7	90.9	82.3	86.4	90.0
	M3ID	6.3	68.8	53.5	5.1	83.0	91.0	82.8	86.7	90.2
	AVISC	6.3	69.0	53.9	5.0	82.8	91.1	82.5	86.6	90.1
	Ours	**4.9**	**71.8**	**44.7**	**3.7**	**84.4**	88.1	**89.2**	**87.1**	**91.1**
Intern VL2	base	8.1	69.6	59.0	5.2	84.0	87.3	**88.8**	88.0	90.0
	RLAIF-V	8.0	68.4	59.3	4.9	84.2	87.7	88.5	88.1	90.1
	VCD	8.5	68.7	58.6	5.0	82.9	87.0	88.4	87.7	89.6
	M3ID	8.4	69.2	58.9	5.4	83.7	86.8	88.4	87.6	89.6
	AVISC	8.4	68.9	59.1	4.8	84.0	87.7	86.8	87.2	89.4
	Ours	**7.9**	**69.8**	**57.8**	**3.7**	**84.7**	**88.2**	**88.8**	**88.5**	**90.3**

D MLLMs Architectures

Tab. 7 shows detailed information about the vision encoder and LLM components of the MLLM architectures used in our experiments.

Table 7: Details of the used MLLM architectures.

MLLMs	Vision encoder	LLM
LLaVA-v1.5 (7B)	CLIP-L-336px	Vicuna-v1.5-7B
LLaVA-v1.5-13B	CLIP-L-336px	Vicuna-v1.5-13B
LLaVA-v1.6	CLIP-L-336px	Vicuna-v1.5-7B
InstructBLIP (7B)	BLIP-2	Vicuna-v1.1-7B
InstructBLIP-13B	BLIP-2	Vicuna-v1.1-13B
mPLUG-Owl2	CLIP-L	LLaMA-2-7B
InternVL2-4B	InternViT-300M-448px	Phi-3-mini-128k-instruct

E Results on MMBench

We further evaluate our method on MMBench Liu et al. (2025). The results in Tab. 8 indicate that our method improves the overall performance and achieves consistent improvements across MLLMs on Coarse Perception (CP). This outcome aligns with the intended effect of our method, as its focus on increasing visual influence is directly linked to improving coarse perception capabilities. For other metrics, our method yields minor improvements due to the possible reason that certain abilities, such as Logical Reasoning (LR), rely more on the language component of MLLMs and cannot be enhanced solely by increasing visual influence.

F Results on MM-Vet

The evaluation on MM-Vet Yu et al. (2023) in Tab. 9 shows that our method achieves consistent overall (Total) improvement, along with enhancements in recognition (Rec) and Optical Character

Table 8: Results on MMBench Dataset.

MLLMs	Method	Overall	CP	FP-S	FP-C	AR	LR	RR
LLaVA-V1.5	base	**62.3**	68.5	**69.6**	**57.7**	73.1	**29.9**	54.7
	ours	61.8	**73.2**	62.6	53.0	**73.3**	27.8	**57.8**
mPLUG-Owl2	base	63.5	68.1	**69.1**	**55.8**	**78.4**	37.0	57.0
	ours	**65.0**	**72.6**	66.6	53.0	76.0	**41.6**	**63.0**

Recognition (OCR), indicating its effectiveness in improving visual recognition. However, its performance varies across other metrics, including knowledge (Know), generalization (Gen), spatial awareness (Spat), and math (Math), suggesting that our method, which focuses on token influence balancing, may not effectively enhance the generalization ability of MLLMs.

Table 9: Results on MM-Vet dataset.

MLLMs	Method	Rec	OCR	Know	Gen	Spat	Math	Total
LLaVA-V1.5	base	32.9	20.1	**19.0**	20.1	**25.6**	5.2	28.0
	ours	**38.9**	2**4.9**	15.0	15.5	24.9	**7.7**	**28.9**
InstructBlip	base	32.4	14.6	16.5	**18.2**	**18.6**	7.**7**	26.2
	ours	**40.5**	**18.0**	**18.7**	17.4	14.9	3.8	**26.6**
mPLUG-Owl2	base	36.1	19.4	**29.8**	19.4	23.9	**7.7**	27.3
	ours	**45.0**	**26.4**	27.9	**25.9**	**24.8**	3.8	**33.9**

G Results on ScienceQA and Vizwiz

We evaluate our method on two complementary multimodal benchmarks. ScienceQA Lu et al. (2022) integrates images, textual context, and curriculum knowledge, requiring models to perform structured multimodal reasoning. VizWiz Gurari et al. (2018), in contrast, consists of visual questions collected from blind users and features real-world challenges such as low-quality images, conversational queries, and unanswerable cases. These datasets jointly assess both reasoning under structured multimodal contexts and robustness in unconstrained real-world settings. As shown in Table 10, our approach consistently improves over the LLaVA-1.5 baseline. These gains demonstrate the effectiveness of our hallucination mitigation strategy in enhancing visual grounding across both knowledge-driven and real-world VQA tasks.

Table 10: Comparison of LLaVA-1.5 and our method on ScienceQA and VizWiz datasets.

MLLMs	Method	ScienceQA(%) ↑	VizWiz(%) ↑
LLaVA-V1.5	base	66.2	48.7
	Ours	**68.7**	**52.8**

H Revisiting the Accuracy–Informativeness Trade-off

In the main paper, we report recall and output length alongside CHAIR scores, since our objective is to evaluate models under a balance of *accuracy* and *informativeness*. This choice is deliberate: our early stopping mechanism can be tuned to shorten responses, which naturally reduces CHAIR scores but at the expense of recall and content richness. Consequently, the trade-off introduced by early stopping is an explicit design choice, and it can be adjusted depending on the requirements of a specific application.

Direct comparison with SOTA methods that omit recall and generation length is therefore not entirely fair. Our analysis confirms that CHAIR scores can drop substantially when outputs are truncated, underscoring the importance of jointly reporting recall and length to present a complete view of performance. Without these complementary metrics, lower CHAIR values may simply reflect shorter, less informative responses rather than genuine improvements in visual grounding. To enable a fairer comparison with prior work, we adjust our early stopping threshold to 12%. Under this setting, our method achieves lower CHAIR scores while maintaining competitive recall, thereby

outperforming both approaches. This demonstrates that our framework not only mitigates hallucination effectively but also preserves informativeness. Moreover, the adjustable nature of the early stopping mechanism ensures that users can flexibly select the optimal balance between accuracy and informativeness for their specific use cases.

Table 11: Comparison with SOTA Methods with 12% Early Stopping Threshold.

MLLM	Method	$C_s \downarrow$	$C_i \downarrow$	R ↑	Len ↑
LLaVA-v1.5	base	48.8	13.4	**78.6**	**99.8**
	PAI Liu et al. (2024c)	24.8	6.9	-	-
	Middle Jiang et al. (2025)	25.0	6.7	-	-
	Ours_ES_12%	**23.5**	**6.5**	55.0	54.1

I Results on MME

Our evaluation on MME Fu et al. (2024) dataset is presented in Tab. 12. Our method achieves better overall (Total) results and equal or improved performance in existence and counting, demonstrating its effectiveness in object recognition. However, it does not improve position accuracy and exhibits varying behavior on color. This diversity may stem from the inherent capabilities of MLLMs, which cannot be solely enhanced through token influence balancing.

Table 12: Result on MME Dataset.

MLLMs	Method	Existence ↑	Count ↑	Position ↑	Color ↑	Total ↑
LLaVA-v1.5	base	190.0	140.0	128.3	155.0	613.3
	ours	190.0	**153.3**	128.3	**163.3**	**634.9**
IntructBLIP	base	180.0	55.0	50.0	130.0	415.0
	ours	**185.0**	55.0	50.0	130.0	**420.0**
mPLUG-Owl2	base	170.0	145.0	73.3	**158.3**	546.6
	ours	170.0	**150.0**	73.3	150.0	**548.3**

J Other Results of POPE

Table 13: More Results on POPE Li et al. (2023b).

Dataset	Setting	Method	LLaVA-v1.5		InstructBLIP		mPLUG-Owl2	
			Acc ↑	F1 ↑	Acc ↑	F1 ↑	Acc ↑	F1 ↑
MSCOCO	Random	base	86.5	84.8	87.1	85.7	86.0	84.4
		ours	**86.8**	**85.1**	**87.9**	**86.8**	**87.9**	**87.1**
	Popular	base	85.5	83.8	84.2	83.6	84.6	83.2
		ours	**85.6**	**84.0**	**85.0**	**84.3**	**86.4**	**85.7**
A-OKVQA	Random	base	88.0	**87.6**	88.5	88.5	86.5	85.7
		ours	**88.1**	87.4	**88.8**	**88.8**	**88.4**	**88.1**
	Popular	base	85.5	85.1	81.9	83.1	82.4	82.2
		ours	85.5	85.1	**82.3**	**83.4**	**85.1**	**85.3**
	Adversarial	base	79.1	79.9	74.8	77.9	74.7	76.9
		ours	**79.5**	**80.1**	**75.3**	**78.2**	**78.2**	**79.9**
GQA	Random	base	88.9	88.2	87.2	87.1	85.2	84.0
		ours	88.9	88.2	87.2	**87.2**	**86.1**	**85.0**
	Popular	base	84.1	84.1	78.6	80.4	78.7	78.5
		ours	**84.2**	84.1	**78.8**	80.4	**81.0**	**80.5**
	Adversarial	base	80.8	81.3	75.9	78.4	76.4	76.8
		ours	**81.1**	**81.6**	**76.1**	**78.5**	**79.2**	**79.1**

We report our experimental results on the POPE dataset, in addition to MSCOCO and adversarial settings, in Tab. 13. The results indicate that our method improves performance across all baseline MLLMs, with more significant gains observed in the adversarial setting. This discrepancy likely arises because adversarial scenarios require models to rely more heavily on visual inputs, aligning with our method's focus on enhancing visual influence. Conversely, for popular and random objects, textual data often provides sufficient statistical information, reducing the necessity for increased visual input reliance.

K Different Sampling Strategies

Tab. 14 presents an ablation study on sampling strategies (non-greedy vs. greedy). We follow the non-greedy sampling setting of VCD Leng et al. (2024), where both top-p and temperature are set to 1. As shown, our method consistently improves performance across both sampling strategies.

Table 14: Ablation Study on Sampling Strategies on POPE MSCOCO Adversarial Dataset.

strategy	Method	LLaVA-v1.5		InstructBLIP		mPLUG-Owl2	
		Acc	F1	Acc	F1	Acc	F1
non-greedy	base	$79.0_{\pm 0.51}$	$81.1_{\pm 0.53}$	$71.6_{\pm 0.49}$	$74.7_{\pm 0.46}$	$71.5_{\pm 0.30}$	$76.6_{\pm 0.28}$
	ours	$\mathbf{82.3}_{\pm 0.27}$	$81.1_{\pm 0.31}$	$\mathbf{82.2}_{\pm 0.29}$	$\mathbf{81.8}_{\pm 0.25}$	$\mathbf{83.2}_{\pm 0.27}$	$\mathbf{82.9}_{\pm 0.26}$
greedy	base	79.4	81.6	79.8	81.4	72.5	77.5
	ours	**83.5**	**82.1**	**82.5**	**82.1**	**84.2**	**83.7**

L Different Model Size

We evaluate our method on different model sizes, 7B and 13B, for LLaVA-v1.5 and InstructBLIP, as shown in Tab. 15. The results indicate consistent improvements across various model sizes. In each model series, the smaller model gets a larger performance boost. With our method, we can achieve high accuracy and detection rates with a smaller 7B model, outperforming a 13B model at its original performance level.

Table 15: Ablation Study on Model Size on LLaVA-QA90 Dataset.

Mothod	LLaVA-v1.5				InstructBLIP			
	7B		13B		7B		13B	
	Acc	Det	Acc	Det	Acc	Det	Acc	Det
base	3.23	3.54	4.78	4.2	3.84	4.07	5.67	4.88
ours	**6.20**	**5.14**	**7.36**	**6.5**	**6.28**	**4.77**	**6.42**	**5.99**

M Gradient Computation Details and Efficiency Ablation

Table 16: Ablation Study on Gradient Methods on the POPE MSCOCO Adversarial Dataset

Methods		Accuracy	F1	Average Speed(ms)
MPLUG-Owl2	IG Enguehard (2023)	83.4	82.9	20335
	direct	84.2	83.7	385

Our method obtains gradients directly through PyTorch's 'torch.autograd.grad' on input tokens, eliminating the need for manual derivations and facilitating straightforward reproduction. For comparison, we evaluate Integrated Gradients (IG) Enguehard (2023); Lundstrom et al. (2022); Kapishnikov et al. (2021) using the SIG Enguehard (2023) implementation; Table 16 presents this ablation.

In the table, "IG" denotes the SIG-based results, while "direct" refers to our torch.autograd.grad approach. Both methods yield comparable accuracy and F1-score, but the direct-gradient variant is substantially more efficient.

N Norm Selection for Token Influence

To evaluate the impact of norm selection on token influence, we study L1 (Manhattan), L2 (Euclidean), and L_∞ (infinity) norms. The L1 norm highlights individual token contributions, while the L2 norm captures overall influence. The L∞ norm focuses on the most dominant token or channel. Results in Tab. 17 show that the L1 norm achieves the best performance, aligning with our intuition that it effectively captures influence magnitude across tokens and channels. In contrast, the L2 norm, by emphasizing overall contribution, can obscure individual token effects, and the L_∞ norm, though capturing the strongest signal, fails to account for the broader token/channel influence.

Table 17: Norm Strategies on POPE MSCOCO Adversarial Dataset.

Norm	LLaVA-v1.5		InstructBLIP		mPLUG-Owl2	
	Acc	F1	Acc	F1	Acc	F1
L1	**83.5**	**82.1**	**82.5**	**82.1**	**84.2**	**83.7**
L2	83.2	81.9	79.5	79.6	83.2	82.9
L_∞	83.4	82.0	82.1	81.8	80.8	80.6

O Hyper parameter Study

Maximum α_m. To determine the optimal maximum amplification factor (α_m) and understand its impact on the model performance, we conducted a search over values from 1 to 6 using the LLaVA-v1.5 model on the POPE dataset for discriminative tasks. For open-ended generation tasks on a subset of the MSCOCO dataset following Deng et al. (2024), we observed garbled text when α_m was set to 5; therefore, we limited our search to values from 1 to 4. As shown in Tab. 18 and Tab. 19, discriminative task on POPE is less sensitive to the value of α_m. The performance on the generative task gets improved while α_m increases but later drops. Therefore, in our experiments, the optimal maximum amplification factor (α_m) is set to 5 and 3 for discriminative and generation tasks, respectively.

Table 18: α_m Study For Discriminative Task On POPE Li et al. (2023b) in MSCOCO Adversarial Setting.

Maximum α_m	1		2		3		4		5		6	
	Acc ↑	F1 ↑	Acc ↑	F1 ↑	Acc ↑	F1 ↑	Acc ↑	F1 ↑	Acc ↑	F1 ↑	Acc ↑	F1 ↑
LLaVA-v1.5	83.4	82.0	83.4	82.0	83.4	82.0	83.4	82.0	83.5	82.1	83.4	82.1

Table 19: Maximum α_m Study For Generation Task on the MSCOCO Subset.

Maximum α_m	1				2				3				4			
	$C_S \downarrow$	$C_I \downarrow$	$R \uparrow$	Len	$C_S \downarrow$	$C_I \downarrow$	$R \uparrow$	Len	$C_S \downarrow$	$C_I \downarrow$	$R \uparrow$	Len	$C_S \downarrow$	$C_I \downarrow$	$R \uparrow$	Len
LLaVA-v1.5	44.0	11.8	76.2	86.1	41.4	11.1	77.4	84.8	41.0	10.9	77.3	85.0	41.4	10.9	77.3	84.9

Early Stopping Threshold. To set the early stopping threshold properly, we conducted a search on a subset of the MSCOCO dataset subset following Deng et al. (2024). Recognizing that the visual influence ratio varies across models, we first analyze the sample-wise visual influence to identify an appropriate range for this study. By searching over the corresponding range, we show results in Tab. 20. These results demonstrate that varying the ES threshold primarily mediates the trade-off between recall and hallucination rate. Our goal is to have balanced recall (R) and instance-level hallucination (C_I), leading us to select thresholds of 7% for LLaVA-v1.5 and LLaVA-v1.6, 25% for InstructBLIP, 2.5% for mPLUG-Owl2 and 10% for InternVL2. We additionally ran an experiment

to measure the ES activation rate using LLaVA-v1.5 with ES threshold 7%. As shown in Tab. 21, ES fires on only 8.7% of the test samples, and when it does, the generated responses are on average just 0.7 tokens shorter. This indicates that ES rarely, and only minimally, truncates outputs.

Table 20: Early Stopping Threshold Study on the MSCOCO Subset

	LLaVA-v1.5				LLaVA-v1.6				IntructBLIP				mPLUG-Owl2				InternVL2			
	6%	7%	8%	9%	5%	7%	9%	11%	15%	20%	25%	30%	2%	2.5%	3%	3.5%	8%	10%	12%	14%
C_S	45.6	41.0	36.6	31.4	29.0	26.0	23.0	17.8	52.6	51.4	47.4	36.0	51.8	45.0	41.2	41.0	37.0	35.2	34.6	32.9
C_I	11.5	10.9	10.2	10.2	8.5	8.1	7.8	7.5	15.0	14.3	13.4	11.7	13.7	12.4	11.0	11.0	8.6	8.1	8.0	7.9
R	79.7	77.3	75.2	70.8	68.5	63.0	58.8	53.0	75.1	74.4	72.3	68.8	77.7	74.9	73.8	73.5	65.8	65.4	65.4	64.0
L_{en}	$92._0$	$85._0$	$75._4$	$63._9$	$119._1$	$101._8$	$81._1$	$62._7$	$107._9$	$103._4$	$93._9$	$74._3$	$89._1$	$83._5$	$78._9$	$77._8$	$180._4$	$175._5$	$170._6$	$162._2$

Table 21: Activation Rate of the Early Stopping on the MSCOCO Subset

Methods		Activate Percentage	Average Length
LLaVA-v1.5 (7%)	base	-	85.1
	ours	8.7%	84.4

P Confidence and Visual Influence

Low confidence often signals potential failure modes in base MLLMs. Here, we demonstrate that our method not only improves accuracy but also increases model confidence. It remains effective even in low-confidence regions for three reasons: 1) We aggregate token gradients at the component level (Eq. 7) rather than using individual token gradients which yields robustness against local gradient noise. 2) We adjust influence towards visual tokens which consistently reduces the hallucination likelihood; 3) Empirically, low model confidence does not correlate with noisy gradients. In our experiments, pretrained MLLMs usually maintain meaningful gradient signals even at low confidence levels. Fig. 6 shows an example where the baseline model mPLUG-Owl2 exhibits low confidence in hallucinated predictions and near-zero confidence in the initial predictions for 'forks' and 'mug'. With GACD, prediction confidence increases alongside the visual influence ratio, with the minimum confidence rising to over 30%.

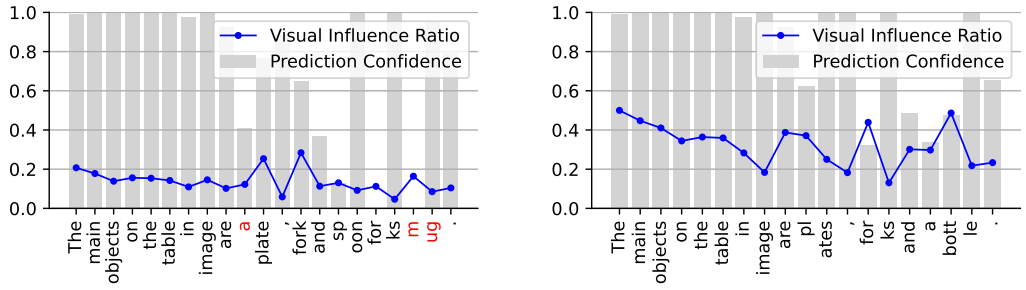

(a) mPLUGOwl2 (b) mPLUGOwl2-GACD

Figure 6: Comparison of prediction confidence with and without GACD. (a) Without GACD, mPLUGOwl2 exhibits low confidence in hallucinated predictions and near-zero confidence in the initial predictions for 'forks' and 'mug'. (b) With GACD, mPLUGOwl2's confidence increases alongside the visual influence ratio, effectively mitigating hallucinations.

Q Question Category Results on the AMBER Dataset

We report discriminative results across different question categories in Tab. 22. Our method improves performance in nearly all categories across all MLLMs. The improvement in InternVL2's object existence is minor, likely due to its already high visual influence ratio. For LLaVA-v1.5

and mPLUG-Owl2, which have lower original visual influence ratios, our method achieves more substantial gains in existence, attribute, and state categories.

Table 22: Results on the Question Categories of Discriminative Task on AMBER Dataset.

Category	Metric	InstructBLIP		LLaVA-v1.5		LLaVA-v1.6		mPLUG-Owl2		Intern-VL2	
		base	ours	base	ours	base	ours	base	ours	base	ours
Existence	acc	70.0	79.8	70.8	93.2	92.9	93.0	75.2	89.9	90.6	90.6
	P	100.0	100.0	100.0	100.0	100.0	100.0	100.0	100.0	100.0	100.0
	R	70.0	79.8	70.8	93.2	92.9	93.0	75.2	89.9	90.6	90.6
	F1	82.3	88.7	82.9	96.4	96.3	96.3	85.8	94.6	95.0	95.0
Attribute	acc	71.9	78.3	72.3	76.1	75.2	77.1	73.9	78.2	82.3	82.6
	P	76.0	81.7	87.3	74.0	74.6	76.4	86.0	76.9	80.9	80.9
	R	64.3	73.0	52.2	82.7	83.0	83.9	57.1	81.8	84.7	85.2
	F1	69.7	77.1	65.3	78.1	78.5	80.0	68.6	79.3	82.8	83.0
State	acc	73.4	76.4	68.2	73.3	78.6	75.2	70.5	77.9	81.2	81.2
	P	75.1	77.1	86.2	70.3	78.6	74.7	84.9	75.5	79.1	78.7
	R	70.6	75.3	43.3	82.0	78.5	82.9	49.8	83.1	84.8	85.5
	F1	72.8	76.2	57.6	75.7	78.5	78.6	62.8	79.1	81.8	82.0
Number	acc	65.4	80.6	75.0	80.1	80.1	80.2	77.8	76.5	82.6	83.3
	P	75.4	93.1	86.9	79.1	79.2	78.6	86.0	77.0	83.0	84.0
	R	45.8	66.2	59.5	82.4	81.7	84.4	66.9	77.0	82.0	82.3
	F1	57.0	77.4	70.6	80.7	80.4	81.4	75.3	77.0	82.5	83.1
Action	acc	79.7	83.7	83.6	82.3	81.9	80.4	84.0	84.1	88.4	88.6
	P	82.5	88.5	92.9	85.9	79.4	81.2	90.9	85.9	86.5	86.8
	R	75.3	77.5	72.7	87.4	86.0	88.6	75.5	85.9	90.9	91.2
	F1	78.7	82.6	81.6	86.6	82.6	84.7	82.5	85.9	88.6	88.9
Relation	acc	62.7	71.9	71.8	61.5	64.5	65.7	70.5	76.9	72.1	77.0
	P	56.2	64.0	65.9	51.9	54.0	56.6	61.0	67.9	60.0	65.1
	R	48.6	73.4	66.3	97.7	95.1	87.2	79.5	83.9	98.3	95.6
	F1	52.1	68.4	66.1	67.8	68.9	68.6	69.0	75.1	74.5	77.5

R Computational Cost

In this section, we analyze the computational cost of the proposed method. On the POPE dataset, our method increases the average computational cost by 101.44% in TFLOPs. This is expected for decoding-based approaches, as they require two forward passes. Importantly, the visual encoder is executed only once, and the second pass processes a limited number of input tokens. Thus, although additional computation is introduced, the overall overhead remains within a practical range.

Table 23: TFLOPs of Baseline vs. Ours with LLaVA-v1.5 on the POPE Dataset.

Method	TFLOPs	Relative Increase
LLaVA-v1.5	9.68	–
Ours	19.49	$+101.44\%$

S Influence Ratio in VQA

Fig. 7 illustrates the visual influence ratio across outputs in VQA tasks, comparing baseline predictions with those obtained after applying GACD. The results confirm that text tokens dominate influence across MLLMs, including InternVL2, which exhibits a relatively high visual influence ratio. As shown in Fig. 3 of the main paper, the overall 60%–100% visual influence ratio across the POPE dataset suggests that visual inputs predominantly determine object existence in VQA tasks. GACD enhances visual influence, effectively balancing text-visual bias. Furthermore, the visualization on InternVL2 demonstrates that the co-occurrence hallucination 'knife' persists despite a high visual influence. GACD successfully eliminates this co-occurrence hallucination.

(a) What are the main objects on the table in the image?

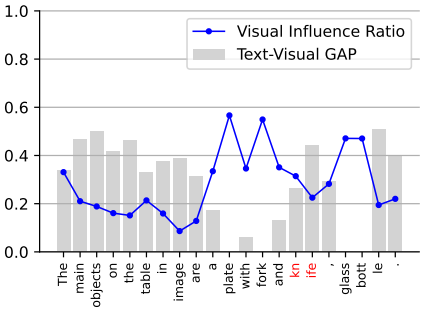

(b) LLaVAv1.5

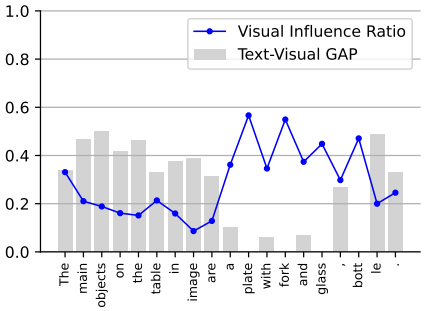

(c) LLaVAv1.5-GACD

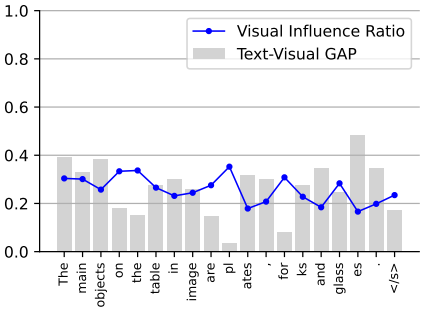

(d) InstructBLIP

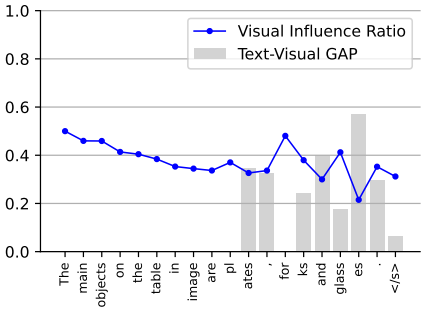

(e) InstructBLIP-GACD

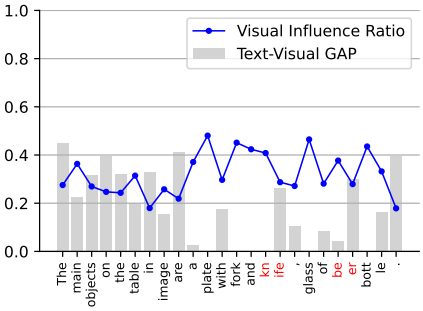

(f) InternVL2

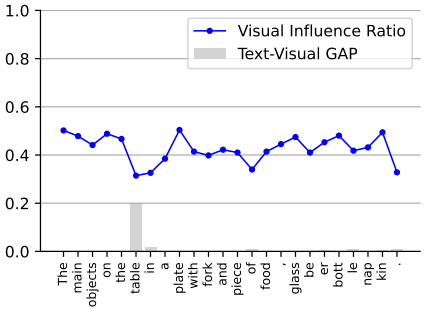

(g) InternVL2-GACD

Figure 7: Influence Ratio across Predicted Tokens in VQA: (left) Baseline predictions; (right) Predictions with GACD. GACD effectively mitigate Text-Visual GAP, balancing text-visual bias. (f) The original InternVL2 shows a dominant visual influence ratio at the hallucinated prediction 'knife', indicating a co-occurrence bias that remains unaddressed even with dominant visual influence. (g) GACD successfully eliminates co-occurrence hallucinations, including 'knife'.

T INFLUENCE RATIO IN IMAGE CAPTION

We further visualize the influence ratio in the image captioning task. Fig. 8 shows that in the baseline LLaVA-v1.5, the influence gap between previous output tokens and visual tokens widens as more

tokens are generated. However, GACD effectively narrows this gap, preventing visual information from being forgotten and thereby reducing hallucinations.

LLaVA: The image features a black dog lying on the floor in a kitchen, resting comfortably on a tiled surface. The dog is positioned near a bowl, possibly enjoying a meal or a snack. In the kitchen, there are several items scattered around. A bottle can be seen on the left side of the dog, while a cup is located closer to the center. A spoon is placed near the right side of the dog, and a bowl is situated on the right side of the scene.

LLaVA-VA: The image features a black dog lying on the floor of a kitchen, resting comfortably on a tile floor. The dog is positioned near a bowl, a toy, and a bag of cat food. The bowl is placed on the floor, while the toy is located closer to the dog.

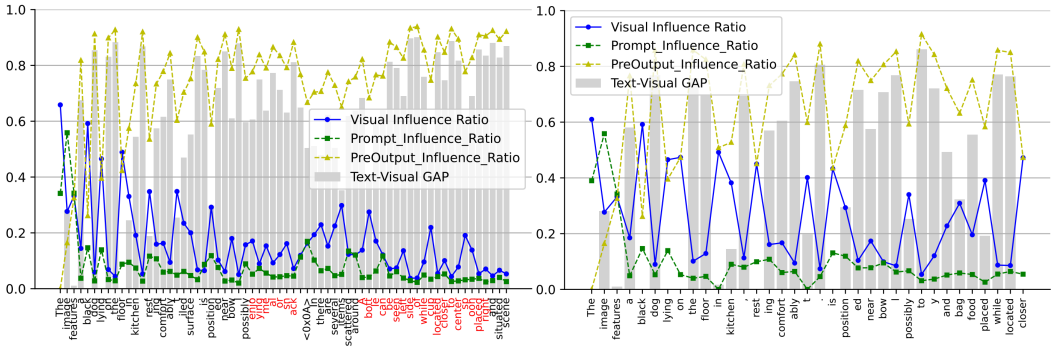

Figure 8: Comparison of influence ratios across predicted tokens with and without GACD. (Left) Without GACD, the influence gap between previous output tokens and visual tokens widens as more tokens are generated. (Right) With GACD, the gap is periodically narrowed to nearly zero, mitigating this trend and reducing hallucination.

U Qualitative Example on Occluded Images

We include a qualitative example in Fig. 9, where a sedan and a building are partially occluded by a white truck, our method prevents the baseline model from hallucinating of persons and vehicles behind the occluding object. This demonstrates our method remains effective on images consisting of occlusions. Image caption w/o Ours: The image features a white truck parked on a city street,

Image caption w/o Ours: The image features a white truck parked on a city street, with graffiti covering its side. The truck is positioned near a crosswalk, and there are several other vehicles in the scene, including a car and a bus. In addition to the vehicles, there are a few people walking around the area.

Image caption w Ours: The image features a large white truck parked on a city street, with graffiti covering its side. The truck is positioned near a crosswalk, and there is another vehicle visible in the background. Additionally, there are buildings in the scene, suggesting an urban setting.

Figure 9: Example of our method applied to an occluded image.

with graffiti covering its side. The truck is positioned near a crosswalk, and there are several other vehicles in the scene, including a car and a bus. In addition to the vehicles, there are a few people walking around the area. Image caption w Ours: The image features a large white truck parked on a city street, with graffiti covering its side. The truck is positioned near a crosswalk, and there is another vehicle visible in the background. Additionally, there are buildings in the scene, suggesting an urban setting.

V Additional Implementation and Experimental Details

Noun tokens are identified using the spaCy library via its `en_core_web_sm` model. For experiments on the Amber dataset Wang et al. (2023), we adopt the original data splits and evaluation metrics. In the MSCOCO Lin et al. (2014) subset, we follow the data partitioning and evaluation protocol of Deng et al. Deng et al. (2024), with splits available in their official repository. For the LLaVA-QA90 Liu et al. (2024b), MME Fu et al. (2024) and POPE Li et al. (2023b) datasets, our setup replicates that of Leng et al. Leng et al. (2024) and use their provided scoring scripts for LLaVA-QA90. Experiments on MMBench Liu et al. (2025), MM-Vet Yu et al. (2023) follow the VLMEvalKit_InternVL2_5 repository. All comparison methods are executed using their official code; we only modify them to enforce greedy sampling and a uniform maximum generation length to align with our experimental settings.

W Limitations and Future Work

Our method is limited to white-box MLLMs, as it requires access to gradients. Its effectiveness depends on the baseline MLLM's original visual influence ratio, and the importance of visual information. As a post-processing technique, our method does not involve model training. In future work, we aim to explore how insights from GACD can guide and improve training strategies for enhanced visual perception in MLLMs.

X Broader Impacts

Our method enhances the factual reliability of multi-modal language models, not only for vision–language tasks but also for modalities such as video and audio, by mitigating hallucinations at inference time. This improvement has several positive societal implications: it can make systems for visual question answering, assistive technologies for the visually impaired, and automated image captioning more dependable, thereby increasing user trust and safety; it can power educational tools that generate accurate descriptions of complex diagrams or historical media, benefiting learners and instructors; and in critical domains such as medical imaging or remote sensing, it can reduce spurious outputs and support more robust decision-making. Conversely, if deployed within surveillance or facial-recognition systems, stronger multi-modal grounding could facilitate more intrusive inferences about individuals from visual data, exacerbating privacy risks.